JOURNAL OF GEOPHYSICAL RESEARCH, VOL. 113, A07S22, doi:10.1029/2007JA012749, 2008

Global MHD simulation of flux transfer events at the high-latitude magnetopause observed by the Cluster spacecraft and the SuperDARN radar system

P. Daum,[1] J. A. Wild,[1] T. Penz,[2] E. E. Woodfield,[1] H. Rème,[3] A. N. Fazakerley,[4] P. W. Daly,[5] and M. Lester[6]

Received 24 August 2007; revised 21 May 2008; accepted 2 June 2008; published 26 July 2008.

[1] A global magnetohydrodynamic numerical simulation is used to study the large-scale structure and formation location of flux transfer events (FTEs) in synergy with in situ spacecraft and ground-based observations. During the main period of interest on the 14 February 2001 from 0930 to 1100 UT the Cluster spacecraft were approaching the Northern Hemisphere high-latitude magnetopause in the postnoon sector on an outbound trajectory. Throughout this period the magnetic field, electron, and ion sensors on board Cluster observed characteristic signatures of FTEs. A few minutes delayed to these observations the Super Dual Auroral Radar Network (SuperDARN) system indicated flow disturbances in the conjugate ionospheres. These "two-point" observations on the ground and in space were closely correlated and were caused by ongoing unsteady reconnection in the vicinity of the spacecraft. The three-dimensional structures and dynamics of the observed FTEs and the associated reconnection sites are studied by using the Block-Adaptive-Tree-Solarwind-Roe-Upwind-Scheme (BATS-R-US) MHD code in combination with a simple open flux tube motion model (Cooling). Using these two models the spatial and temporal evolution of the FTEs is estimated. The models fill the gaps left by measurements and allow a "point-to-point" mapping between the instruments in order to investigate the global structure of the phenomenon. The modeled results presented are in good correlation with previous theoretical and observational studies addressing individual features of FTEs.

Citation: Daum, P., J. A. Wild, T. Penz, E. E. Woodfield, H. Rème, A. N. Fazakerley, P. W. Daly, and M. Lester (2008), Global MHD simulation of flux transfer events at the high-latitude magnetopause observed by the Cluster spacecraft and the SuperDARN radar system, *J. Geophys. Res.*, *113*, A07S22, doi:10.1029/2007JA012749.

1. Introduction

[2] The major process by which energy, mass, and momentum are transferred from the solar wind into the magnetosphere is magnetic reconnection at the dayside magnetopause. The process of reconnection allows interplanetary magnetic flux tubes to couple with those in the magnetosphere [*Dungey*, 1961] and enables plasma from the solar wind and magnetosheath to enter the magnetosphere along the newly joined flux tubes. Assuming time-varying reconnection of the interplanetary magnetic field (IMF) and the Earth's magnetic field, the motion of these flux tubes result in disturbances in the surrounding magnetic field. The first signatures of open flux tube motion and their associated disturbances were seen by *Haerendel et al.* [1978] in magnetic field data from the HEOS-2 spacecraft, and by *Russell and Elphic* [1978, 1979] in the ISEE-1 and -2 data who termed them "flux transfer events" (FTEs). These first observational studies showed that the peculiar magnetic field signatures of FTEs were bipolar perturbations in the component normal to the magnetopause boundary and an enhancement of the overall magnetic field strength. The early physical interpretation of these FTEs were L-shaped flux tube structures produced by patchy and impulsive reconnection near the subsolar magnetopause. These tubes have a strong curvature where they cross the magnetopause and they are dragged poleward (dependent upon B_z IMF) and along the equatorial flanks (dependent upon B_y IMF) over the magnetopause due to magnetic tension and magnetosheath flows. Additional studies by *Berchem and Russell* [1984], *Russell et al.* [1985], and *Kawano and Russell* [1996, 1997] indicate that FTEs are signatures of nonsteady patchy magnetic reconnection which are formed at the dayside magnetopause and travel around the mag-

[1]Department of Communication Systems, Lancaster University, Lancaster, UK.
[2]Osservatorio Astronomico di Palermo, INAF, Palermo, Italy.
[3]Centre d'Etude Spatiale des Rayonnements, Toulouse, France.
[4]Department of Space and Climate Physics, Mullard Space Science Laboratory, University College London, Dorking, UK.
[5]Max Planck Institute for Solar System Research, Katlenburg-Lindau, Germany.
[6]Department of Physics and Astronomy, University of Leicester, Leicester, UK.

0148-0227/08/2007JA012749$09.00

netopause in an antisunward direction. Later studies focusing on particle observations showed that FTEs can also be characterized by a mixture of magnetosheath and magnetospheric plasma [*Daly et al.*, 1981; *Scholer et al.*, 1982; *Paschmann et al.*, 1982; *Thomsen et al.*, 1987].

[3] There have been many papers presenting observational features of FTEs (see, for example, *Elphic* [1995] and *Lockwood and Hapgood* [1998] for reviews of FTE observations and their interpretation), but there exist only a limited number of studies on the motion and configuration of FTEs, including both modeling and observations [e.g., *Cowley and Owen*, 1989; *Berchem et al.*, 1995; *Fedder et al.*, 2002; *Cooling et al.*, 2001; *Kawano and Russell*, 2005; *Pu et al.*, 2006; *Robert et al.*, 2006; *Fear et al.*, 2007]. Most recently, case studies by *Hasegawa et al.* [2006] (reconstruction study) and *Raeder* [2006] (modeling study) have shown the anatomy and formation process of these unsteady reconnection patches. The two studies concluded that in their cases the unsteady reconnection patches were a result of sequentially generated X-lines which then form dual or multiple X-lines [*Lee and Fu*, 1985, 1986; *Fu and Lee*, 1986] with a ''quasi-periodicity'' [*Rijnbeek et al.*, 1984; *Lockwood and Wild*, 1993; *Neudegg et al.*, 2000] caused by the convection and reformation time [*Raeder*, 2006] of the flux tubes.

[4] The magnetic footprints of newly opened flux tubes are connected to the Northern and Southern Hemispheres, respectively, and can be observed using ionospheric high-frequency (HF) coherent-scatter radars. FTEs produce ionospheric disturbances caused by electron density irregularities which drift with the newly opened flux tubes over the auroral regions [*Provan et al.*, 2002; *Marchaudon et al.*, 2004]. These events are observed by ionospheric radars as high velocity antisunward transient flows which are interpreted as the response to transient magnetopause reconnection [*Pinnock et al.*, 1993, 1995; *Rodger and Pinnock*, 1997]. Studies by *Provan et al.* [1998] and *Provan and Yeoman* [1999] showed quasi-periodic sequences of these observations termed ''pulsed ionospheric flows'' (PIFs), these are also often seen as poleward-moving regions of enhanced backscatter power termed ''poleward-moving auroral radar forms'' (PMRAFs). These radar forms are widely accepted to be the auroral counterparts of FTEs [e.g., *Sandholt et al.*, 1990; *Thorolfsson et al.*, 2000]. The enhancement in the backscatter power is caused by electron density irregularities which are provoked by plasma particles gyrating down the flux tubes whilst they are still dragged over the magnetopause. Since the flux tubes connect two points in space, it is evident that only coordinated ground- and space-based studies can describe the large-scale dynamics and structure of FTEs over a large spatial region.

[5] *Elphic et al.* [1990] presented the first simultaneous observation of FTEs seen by the European Incoherent Scatter (EISCAT) radar system and the ISEE-1 and -2 spacecraft. In a further study *Neudegg et al.* [1999] presented a coordinated space- and ground-based study of FTEs using magnetometer data from the Equator-S spacecraft and radar data obtained from several radars belonging to the Super Dual Auroral Radar Network (SuperDARN) operating in a high temporal and spatial resolution mode. Following these single spacecraft conjunction studies, *Wild et al.* [2001] presented the first concurrent study of FTEs using multipoint measurements taken by the quartet of the ESA Cluster spacecraft in conjunction with measurements from the Co-operative UK Twin-Located Auroral Sounding System (CUTLASS; two UK operated radars which are part of the SuperDARN network) and the EISCAT radar systems. The simultaneous in situ measurements taken by the four identical Cluster spacecraft allowed Wild and coworkers to study the characteristics of the FTEs for the first time with spatial and temporal information. *Wild et al.* [2001] showed that the Cluster and CUTLASS signatures were closely related and provide a direct indicator for mass, energy, and momentum transfer into the magnetosphere-ionosphere system resulting from pulsed reconnection sites as originally outlined by *Dungey* [1961]. In a further study *Wild et al.* [2003] showed that the CUTLASS observations of the Northern Hemisphere ionosphere are closely correlated with similar SuperDARN observations in the Southern Hemisphere ionosphere. On the basis of a comparison of both hemisphere observations *Wild et al.* [2003] concluded that the observations must have been actuated by either a single X-line extending over several hours magnetic local time (MLT) in the prenoon and postnoon sectors of the magnetopause or by multiple X-lines with a similar azimuth displacement in the high latitudes.

[6] A subsequent theoretical study of the time period from 0915 to 1115 UT on the 14 February 2001 undertaken by *Penz et al.* [2006a, 2007] showed that by using the Cagniard-deHoop method [*Cagniard*, 1962; *De Hoop*, 1960, 1961; *Heyn and Semenov*, 1996] they could reconstruct the electric field of the reconnection site based upon the magnetic field measurements from Cluster. By using this method, Penz and coworkers calculated time series of the electric field by performing the analytical inverse Laplace transform of the Petschek-type model of reconnection.

[7] From these theoretical considerations they also inferred the distance of the reconnection sites from the spacecraft. Penz and coworkers [*Penz et al.*, 2006a; *Penz*, 2006] showed that the observed magnetospheric FTEs were caused by a reconnection site located $4.0 \pm 2.1\ R_E$ from the Cluster formation and that the FTEs observed in the magnetosheath were caused by a reconnection site located $3.7 \pm 1.5\ R_E$ away from the Cluster formation. *Penz et al.* [2007] further showed that the observed FTEs described by *Wild et al.* [2001, 2003] were caused by reconnection bursts lasting about 2.6 ± 0.9 min.

[8] The next step in this line of investigations is presented in this paper. We recap briefly the simultaneous observation of the FTE signatures by the Cluster spacecraft and by the SuperDARN radars to constrain the spatial and temporal evolution of the observed features and then compare these observations with a global MHD simulation to fill the gaps left by the point measurements.

[9] This combination of measurements with a global simulation allows us for the first time to address in one study several features of FTEs which have been separately discussed in earlier investigations. Most significantly, the observational features addressed by *Wild et al.* [2001, 2003] and *Penz et al.* [2006a, 2007] can now be shown in a three-dimensional large-scale context. Also the isolated features of FTEs pointed out in previous global MHD simulation studies by *Fedder et al.* [2002] and *Raeder* [2006] can now

be put into context with concurrent space- and ground-based observations.

[10] The study presented here builds upon the initial survey of *Berchem* [2000] who showed the advantages of the synergy of multipoint measurements from space- and ground-based instruments combined with global MHD simulations. Preliminary results for the interval of interest (first presented by *Daum and Wild* [2006]) are extended in order to present a unique mapping between the points of observation exploiting a high-resolution MHD simulation. This high-resolution data allows us to model a wide range of observational features of the FTEs from small to large scales in order to study the general dynamics of the phenomenon.

2. Instrumentation

[11] The modeling study undertaken in this paper is based upon a global MHD simulation of the geospace environment in order to link FTE observations from ground- and space-based instruments on the 14 February 2001 in the time from 0930 UT to 1100 UT. The analysis techniques and the ground- and space-based experiments for the time of interest are described in detail by *Wild et al.* [2001, 2003] and *Wilken et al.* [2001] (discussed FTE observation from 14 January 2001; orbital configuration, instrument setting, and observations were very similar to the ones presented here) and the references therein. Therefore in this section we shall only briefly summarize the instruments employed.

[12] We shall first address the main characteristics of the space-based instruments followed by the main characteristics of the ground-based instruments employed. This division also represents the ''upper/lower layer'' mapping structure utilized in the upcoming sections for combining the global MHD simulation with the observations.

[13] The space-based data presented in this study were obtained from the Cluster fluxgate magnetometer (FGM) experiment [*Balogh et al.*, 1997, 2001], the Cluster Ion Spectrometry (CIS) experiment [*Rème et al.*, 1997, 2001], the Cluster Plasma Electron and Current Experiment (PEACE) [*Johnstone et al.*, 1997; *Owen et al.*, 2001], and the Research with Adaptive Particle Imaging Detectors experiment (RAPID) [*Wilken et al.*, 1997, 2001].

[14] The main ground-based observations were obtained from the SuperDARN radar systems [*Greenwald et al.*, 1995] in the Northern and Southern Hemispheres. The main focus herein lies on the Northern Hemisphere radar at Hankasalmi (Finland) and for comparison the Southern Hemisphere radar located near the Syowa station (Antarctica). In order to estimate the large-scale ionospheric flow patterns, multiple radar stations have been employed to create convection maps using the ''map-potential'' method developed by [*Ruohoniemi and Baker*, 1998].

2.1. Space-Based Instrumentation

[15] The quartet of ESA Cluster spacecraft [*Escoubet et al.*, 2001] were launched in July/August 2000 into a highly elliptical orbit (19.6 (apogee)/4.0 (perigee) R_E). The orbital plane is fixed in the inertial frame of the Earth, therefore the apogee processes through 24 h of local time (LT) with a 12 month periodicity. The four spacecraft typically have a tetrahedral configuration near the magnetopause. The spacecraft formation allowed for the first time simultaneously three-dimensional spatial and temporal studies of the geospace environment.

[16] In Figure 1 we show the projection of the orbital path of Cluster 1 (Rumba) onto the $\mathbf{x}-\mathbf{z}$ and $\mathbf{x}-\mathbf{y}$ Geocentric Solar Magnetospheric (GSM) reference planes in the principal period of interest from 0930 to 1100 UT on the 14 February 2001, when the spacecraft were in a radial distance of 11.18–12.46 R_E from the Earth at the vicinity of the magnetopause. The satellite separation during the time of interest varied from 530 to 590 km. A close up of the formation can be seen in the insets of Figure 1. The solid gray lines indicate the modeled magnetopause shape after *Shue et al.* [1997] and the dashed lines indicate the modeled bow shock shape and location after *Bennett et al.* [1997]. The interval of interest corresponds to an outbound pass through the postnoon high-latitude magnetopause with an actual crossing of the magnetopause region in the time from 1017 to 1031 UT.

[17] A characteristic observational feature of FTEs is the highly structured bipolar signature in the magnetic field component normal to the magnetopause and an increase in the total magnetic field strength. In order to show these features we utilize data from the FGM instrument onboard the Cluster spacecraft analyzed at 4 s resolution (corresponding approximately to a spin of the spacecraft). *Wild et al.* [2001] showed that the observations made by the other three spacecraft are similar to those taken by Cluster 1 so that we concentrate here only on the observations made by the FGM on board Cluster 1 to identify the magnetic field FTE characteristics. Later in section 5 (Model results) data from all four spacecraft are used to examine the electric current density using the so-called curlometer technique [*Dunlop et al.*, 1988], while high-resolution FGM data with up to 67 vectors/s are used to examine the velocity of the FTE structure moving over the Cluster formation.

[18] Another feature associated with FTEs is the mixture of particles of magnetospheric and magnetosheath origin [*Thomsen et al.*, 1987; *Smith and Owen*, 1992]. This study therefore employs particle measurements taken by the CIS, PEACE, and RAPID instruments on board Cluster 1. For the determination of the ion population, data from the Hot Ion Analyzer (HIA, CIS-2) which is part of the CIS experiment was utilized. The CIS data shown below are retrospectively generated spectrograms from the full three-dimensional ion distribution of the HIA instrument in high-sensitivity, solar wind, magnetospheric mode acquired over three spins of the spacecraft. The electron plasma observations have been obtained from the PEACE and RAPID instruments. The PEACE instrument is designed to make observations of the Cluster spacecraft low- and high-energy electron environment. The observations shown below represent the spectrum of the High Energy Electron Analyzer (HEEA) sensor of the PEACE instrument averaged over all look directions in a temporal resolution of 4 s in an energy range of 30 eV to 26 keV. The other electron measurements are taken from the RAPID instrument, this detector provides an analysis of the suprathermal plasma distribution in the energy ranges from 20 to 400 keV. The data shown below are retrospectively generated from the observations made by the Imaging Electron Spectrometer (IES) at 4 s resolution

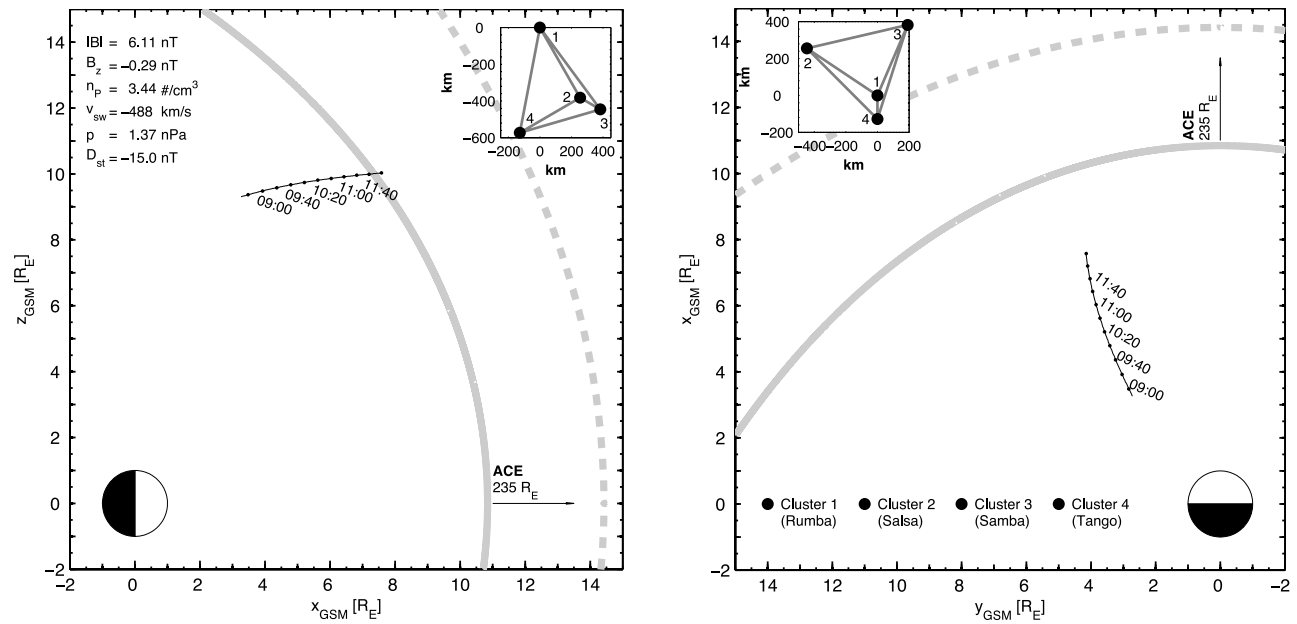

Figure 1. Plots showing the (left) **x**–**z** and (right) **x**–**y** projection of the Cluster 1 (Rumba) orbit in a GSM reference frame on the 14 February 2001 in the time range 0830–1200 UT adjacent to the magnetopause. The modeled magnetopause shape [*Shue et al.*, 1997] is shown by the solid gray lines, and the modeled bow shock [*Bennett et al.*, 1997] shape is indicated by the dashed lines. The models are parameterized by the solar wind parameters shown in Figure 1 (left) in upper left-hand corner. The solar wind data are obtained from the ACE satellite and lagged by ∼55 min. The two insets show the other Cluster spacecraft in relation to Cluster 1 at 1046 UT (time of predominant FTE observation discussed in section 3); the insets show the actual tetrahedral formation and separation in km as projection onto the related planes.

from eight different energy channels in the nine polar directions of the RAPID instrument.

2.2. Ground-Based Instrumentation

[19] The SuperDARN system comprises a network of similar ground-based coherent-scatter radars that operate in the HF band. The network of radars and their fields of views (FOV) cover large parts of the Northern and Southern Hemisphere polar ionospheres. In this section we only outline the most important characteristics of the radar system utilized in this study and refer to *Chisham et al.* [2007] for a detailed overview of the radar system, observational techniques and data analysis methods.

[20] Figure 2 shows the geographical position and FOV of the main radar system employed in this study in the Northern Hemisphere. Overlaid in Figure 2 are the magnetic footprints of the Cluster 1 spacecraft traced to 100 km altitude obtained from the MHD simulation runs. To highlight the evolution of the footprint in time, the footprints are gray scale coded in time for every 5 min. The black numbered solid dots indicate the footprint location at the time of observed FTE features.

[21] The Finland radar is located at Hankasalmi (62.3°N, 26.6°E; it is one part of the two CUTLASS radars), like most SuperDARN radars it is operated in the HF frequency band from 8 to 20 MHz and uses a phased array system of antennas to transmit HF radio pulses (commonly between 10 and 14 MHz) into the ionosphere. The phased array systems of the SuperDARN radars result in 16 virtual beams within the ∼52° FOV, with each beam subdivided into 75 range gates. At the time of interest, the Finland radar was operating with range gates of 45 km, a range to the first gate of 180 km and a 3 s dwell time at every beam location. Thus, a full scan of all 16 beams was performed every 1 min resulting in a complete FOV coverage of over 3000 km in range and a temporal resolution of 1 min. The radar measures the backscatter power from electron irregularities in the *E* and *F* regions of the ionosphere. Since *F* region electron density irregularities drift at the **E** × **B** velocity, the ionospheric motion observed by the radar represent a direct indicator of the motion of newly opened flux tubes.

[22] The process can be briefly described as follows; at the reconnection site magnetospheric flux tubes merge with those in the magnetosheath allowing plasma flow between the magnetosheath and magnetosphere. The charged particles of the plasma then gyrate down the newly opened magnetic field lines while at the same time, the footprint of these field lines move toward the pole due to the magnetic tension imposed on the field lines at the magnetopause. Since the charged particles are "frozen" to the magnetic field lines they follow this drag motion. As a result, the **E** × **B** motion can be measured by the radar systems and can be seen as so-called PMRAFs in the radar backscatter measurements.

[23] From the backscattered signal the Doppler spectra can be obtained via autocorrelation functions. This analysis technique also allows the line of sight (LOS) Doppler velocity of the ionospheric plasma to be derived. The FTE signatures in the radar measurements can be described as transient increases in the LOS velocity propagating poleward.

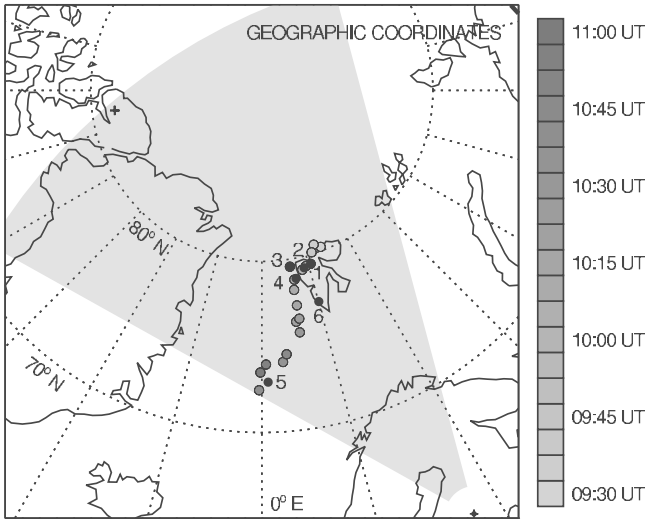

Figure 2. Plot showing the geographical coverage (gray area) of the Finland SuperDARN radar (located at Hankasalmi 62.3°N, 26.6°E; part of the CUTLASS radar system) as well as the magnetic footprint of Cluster 1 at an altitude of 100 km. The traces were done by using the high-resolution MHD simulation at 5 min intervals. The footprints are gray scale coded in time in accordance with the key to the right. The black numbered dots represent the magnetic footprint location at the time of the observed FTEs. The numbers are according to the order of observation 0945 UT (1), 0953 UT (2), 0959 UT (3), 1004 UT (4), 1042 UT (5), and 1046 UT (6).

[24] Whilst only the Northern Hemisphere is presented in Figure 2, conjugate observations are obtained from the Syowa East radar (69.0°S, 39.6°E) in Antarctica. In addition to the mesoscale (hundreds of kilometers) convection observations made by the Finland and Syowa East radars, observations from all available SuperDARN radars in the Northern Hemisphere have been used to produce large scale (thousand of kilometers) convection maps of the Northern Hemisphere ionosphere. These maps are then compared to the space-based observations exploiting the MHD simulation data to achieve three-dimensional point-to-point mappings. The comparison is then used to show the one-to-one correlation between the space- and ground-based observation as originally outlined by *Wild et al.* [2003].

3. In Situ Observations

[25] The study presented here focuses on the large-scale modeling of a series of FTEs observed by the Cluster spacecraft in the high-latitude magnetopause in combination with observations of the conjugate ionospheric flows made by HF radar systems in the Northern and Southern Hemisphere, respectively, on 14 February 2001 between 0930 and 1100 UT. The main focus of this study is to infer the behavior of the FTE structures in the regions between the available measurements by using a global MHD simulation. The global MHD simulation fills the gaps left by measurements and allows us to establish causal relationships between the point measurements taken by the instruments.

[26] The MHD simulation is driven by real IMF conditions; therefore we shall first present the upstream IMF and solar wind conditions which were obtained from the Advanced Composition Explorer (ACE) satellite [*McComas et al.*, 1998; *Smith et al.*, 1998; *Stone et al.*, 1998]. These upstream observations determine the inflow upstream boundary conditions for the Block-Adaptive-Tree-Solarwind-Roe-Upwind-Scheme (BATS-R-US) MHD simulation. Second, we shall present briefly the in situ field and plasma observations drawn from the Cluster 1 spacecraft which arose from the interaction of the solar wind with the magnetosphere, followed by highlighted features of the ground-based observations of the ionospheric flows which subsequently arose from the FTEs seen by Cluster in the vicinity of the magnetopause.

3.1. Upstream Solar Wind Observations

[27] The global MHD simulation is driven by real upstream solar wind conditions. Figure 3 presents an overview of the solar wind and IMF observations made by the Solar Wind Electron, Proton, and Alpha Monitor (SWEPAM) and the Magnetic Field Experiment (MAG) on board the ACE satellite, located some 235 R_E upstream from the Earth during the interval of interest. Figure 3a shows the solar wind density followed by the solar wind velocity and magnetic field strength components in a GSM reference frame. Figure 3h shows the IMF clock angle defined as $\arctan(B_y/B_z)$. During the interval of interest, the IMF was predominantly southward (B_z negative) and duskward (B_y positive) with a corresponding negative clock angle.

[28] The solid black traces in Figure 3 present the ACE measurements projected to the subsolar magnetopause with a propagation delay calculated for each measurement (calculated using the technique of *Khan and Cowley* [1999]; taking into account the propagation of IMF features with the solar wind to the bow shock and then across the magnetosheath to the magnetopause), the average of these lag times was ~55 min.

[29] The light gray traces with round markers present the same measurements but propagated to 33 R_E taking into account the propagation of IMF features with the solar wind in free space which lead to an average lag time of ~43 min. This propagation boundary of 33 R_E represents the BATS-R-US inflow upstream boundary conditions for the resistive MHD equations. The markers represent the 1 min timing intervals at which the MHD run was computed. At the other boundaries the BATS-R-US model assumes a zero gradient for the plasma variables since these boundaries are far enough from Earth that they have no significant effect on the dynamics due to the fact that they introduce a negligible effect in the resistive MHD equations describing the domain.

[30] In addition to the propagated density, shown in Figure 3a, also the 50% decrease of the original value (dark gray trace with square markers) is shown and used as a constrained upstream inflow boundary condition for the BATS-R-US run. This 50% decrease arose from different simulation runs computed with different densities varying from 100% to 30% of the original value, this was necessary since a comparison of a 100% density MHD run with the Cluster observations showed that in the simulation the GSM B_y component turned positive earlier than indicated by the Cluster data. This indicates that the boundary layer is pushed to a lower radial position as observed in the real data and that the model overestimates the pressure influence.

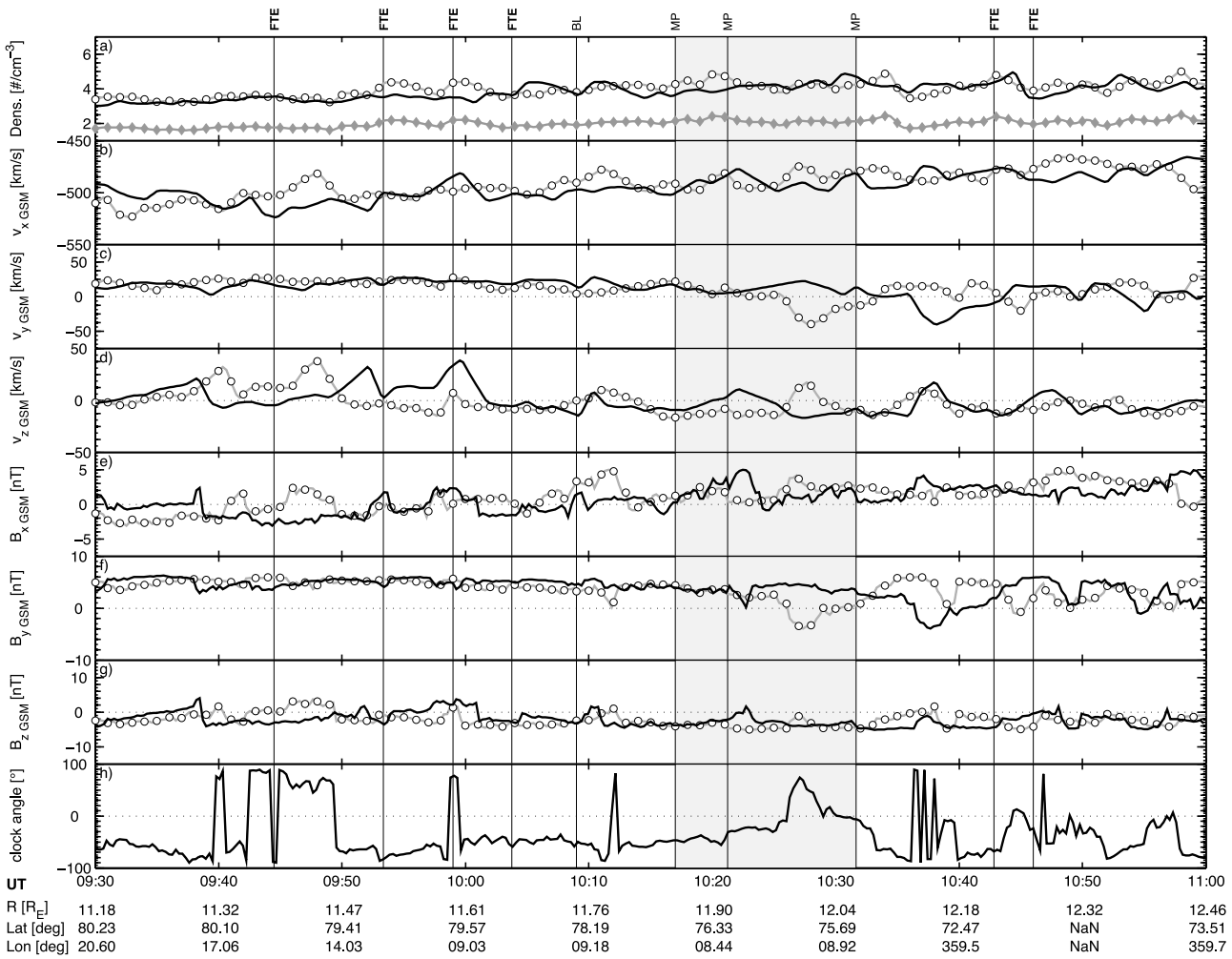

Figure 3. Solar wind (model input) measurements from the ACE satellite between 0930 and 1100 UT (lagged time). The solid black traces indicate the in situ observations made by ACE at 16 s resolution. Each point is lagged individually to the SSP point using the technique of *Khan and Cowley* [1999]. The average lag time corresponds to ~55 min as originally outlined by *Wild et al.* [2001]. The light gray traces represent the measurements projected to 33 R_E (lagged by ~43 min) as upstream input boundary conditions for the BATS-R-US simulation, the dots represent the minute intervals of the simulation outputs. (a) The solar wind density, with the darker gray trace representing the 50% decrease of the solar wind density used in the model runs. (b)–(d) The GSM v_x, v_y, v_z components of the solar wind and (e)–(g) the GSM B_x, B_y, B_z components of the interplanetary magnetic field. (h) The IMF clock angle (defined as $\arctan(B_y/B_z)$). The FTEs discussed in the text are indicated by solid vertical lines and labeled "FTE"; encounters with the boundary layer and magnetopause are labeled as "BL" and "MP," respectively. The *x* labels show in addition to UT the radial distance of Cluster 1 from the Earth and the geographical latitude and longitude of the magnetic footprint obtained from the MHD run.

[31] In constraining the MHD model by decreasing the plasma density and comparing the shape and location of the resulting magnetopause with different magnetopause models [see *Šafránková et al.*, 2002, and references therein] as well as with a wide range of Cluster data (M. Denton, submitted manuscript, 2008) it was possible to constrain the location of the magnetopause boundary layer position in the BATS-R-US run, so that it is coincident with the Cluster observation at ~1009 UT [*Daum and Wild*, 2006]. The comparison between the *Shue et al.* [1997] magnetopause boundary model and the constrained BATS-R-US simulation data can be seen in the following sections.

3.2. Cluster/SuperDARN Radar Observations

[32] Figure 4 presents a summary of the Cluster 1 magnetic field and plasma measurements first discussed by *Wild et al.* [2001] as well as highlighted observational features of the ground-based radar systems discussed by *Wild et al.* [2003].

[33] Figure 4 (first panel) and Figure 4 (second panel) show Cluster 1 FGM data at 4 s resolution transformed into boundary normal coordinates using a minimum variance analysis [*Sonnerup and Cahill*, 1967; *Russell and Elphic*, 1978]. Figure 4 (first panel) shows the variations in B_N, the magnetic field component in the direction normal to the

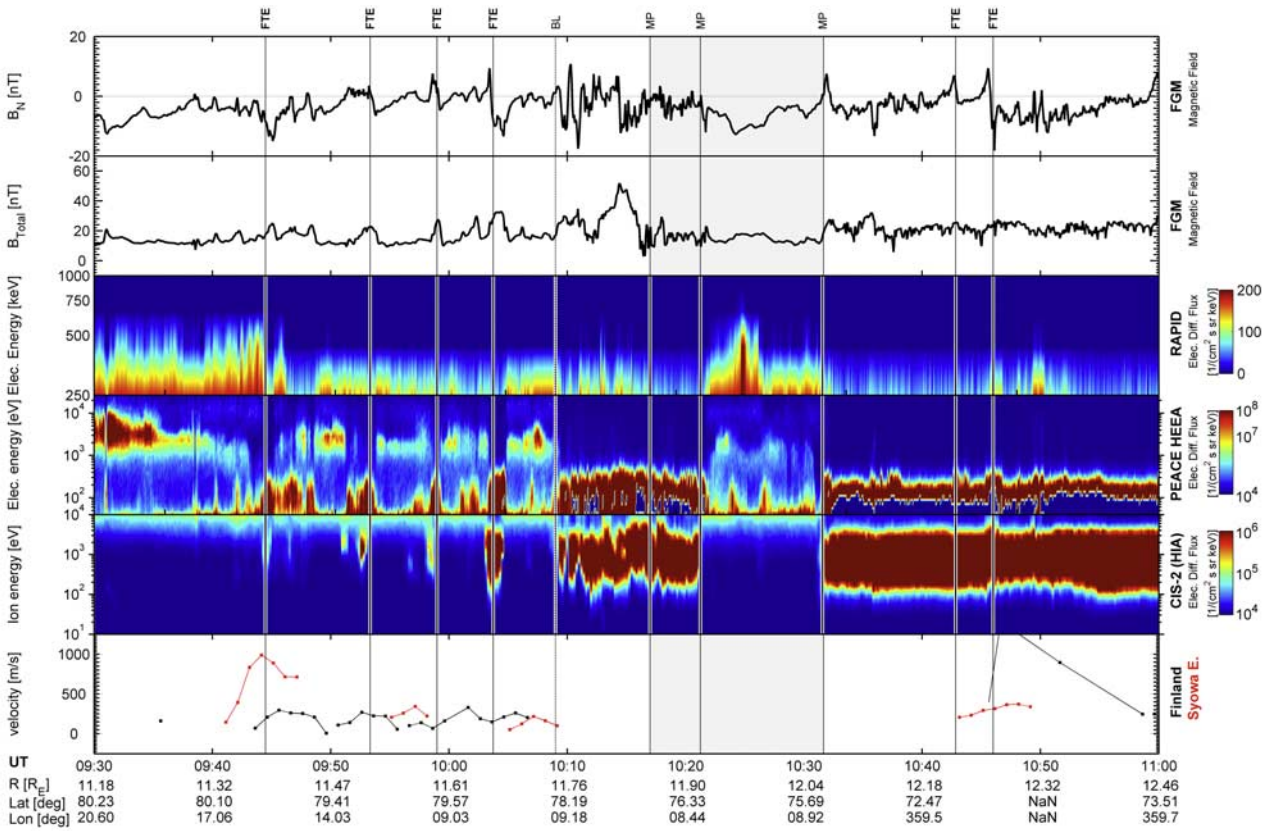

Figure 4. Cluster spacecraft observations and SuperDARN radar observations for the interval of 0930–1100 UT on 14 February 2001. The first and second panels show the magnetic field component B_N normal to the magnetopause and the total magnetic field strength obtained from the B_L, B_M, and B_N components of the boundary-layer coordinate system [*Russell and Elphic*, 1978]. The third and fourth panel represent the electron energy distribution measured in the field-parallel direction by the RAPID and PEACE HEEA instrument onboard Cluster 1. The fifth panel shows the ion energy distribution over all pitch angles observed by the CIS2 (HIA) instrument. The sixth panel shows the mean velocity of the Finland beam 3 and Syowa East beam 0 averaged over ~74.5°–76.0°N and ~74.5°–76.0°S magnetic latitude, respectively. The FTEs discussed in the text are indicated by solid vertical lines and labeled "FTE" (at 0945 UT, 0954 UT, 0959 UT, 10 04 UT, 1042 UT, and 1046 UT) encounters with the boundary layer and magnetopause crossings are labeled as "BL" (at 1009 UT) and "MP" (at 1017 UT, 1021 UT, and 1031 UT), respectively.

magnetopause, while Figure 4 (second panel) shows the total magnetic field strength.

[34] Figure 4 (third panel) and Figure 4 (fourth panel) show the electron energy-time spectrograms from the RAPID and PEACE instrument, respectively, measured in the field-parallel direction. Figure 4 (fifth panel) shows the ion energy-time spectrogram obtained from the CIS instrument over all pitch angles. Figure 4 (sixth panel) shows the low-latitude scatter measurements of the Finland and Syowa radars averaged over ~74.5°–76.0°N and ~74.5°–76.0°S magnetic latitude, respectively.

[35] The magnetic field and particle measurements clearly indicate the observation of four magnetospheric FTEs at 0945 UT, 0954 UT, 0959 UT, 1004 UT, indicated in Figure 4 by the vertical lines labeled "FTE" followed by a boundary layer encounter (marked as "BL") at 1009 UT associated with increasingly variable field and plasma observations which culminate in three magnetopause crossings (marked as "MP") at 1017 UT, 1021 UT, and 1031 UT. Following the entry of Cluster 1 into the magnetosheath at 1033 UT further FTEs were observed at 1042 UT and 1046 UT. All FTE observations are associated with a clear bipolar signature in the B_N component and an increase of the overall field strength. During the magnetospheric FTEs the ion and electron energy distributions of the PEACE, CIS, and RAPID instruments indicated the appearance of magnetosheath-like energy distributions (increasing ion flux in the 10^2–10^3 eV range and increasing electron flux in the 10^2–10^3 eV range accompanied by the disappearance of electrons in the 10^3–10^4 eV range). The later magnetosheath FTE observations by the PEACE, CIS, and RAPID instruments show a slight energization of the magnetosheath plasma and possibly (at 1046 UT) evidence for escaping magnetospheric electrons in the low 250–300 keV range of the RAPID instrument. This characteristic mixing of magnetosheath and magnetospheric ions and electrons indicates the joining of magnetosheath and magnetospheric magnetic flux tubes. This reconnection process enables magnetosheath plasma to enter the magnetosphere and vice versa. This effect can also be observed in the PEACE and RAPID

instruments in the dropouts of the higher-energy electrons and appearances of patches of lower-energy electrons. We note that the exact nature and duration of the observations varied between the FTEs.

[36] Combining the observations in Figure 4 (first panel) and Figure 4 (fifth panel), it should be noted that the significant features of the FTEs became more prominent as the spacecraft approached the magnetopause. This is consistent with the studies undertaken by *Penz et al.* [2006a, 2007], where the currently discussed FTEs have been analyzed using a novel model [*Semenov et al.*, 2005; *Penz et al.*, 2006b] which is based on the assumption of time-dependent Petschek-type reconnection. By applying this model to the in situ magnetic field data obtained from the FGM instrument it was possible to obtain the temporal variations of the reconnection field responsible for each FTE and subsequently also the normal and tangential distances of the reconnection sites from the spacecraft. Penz and coworkers concluded that the FTEs observed must have been produced by reconnection sites in close proximity to the Cluster formation. Furthermore, their results suggested that the magnetospheric FTEs observed by Cluster, before the first boundary layer encounter at 1009 UT, were produced by reconnection sites at normal distances from the Cluster satellites ranging from 0.9 R_E (for the FTE observed at 0945 UT) to 0.5 R_E and 0.3 R_E (for the later examples) and tangential distances of $\sim 4.0 \pm 2.1$ R_E [*Penz*, 2006]. These results are consistent with the observations made by Cluster (see Figure 4) which show that the characteristic features of the FTEs became clearer as closer the spacecraft were approaching the magnetopause. The predominant observational signatures of an FTE can be seen at 1046 UT in the space-based as well as in the ground-based instruments. We shall therefore utilize this example to study more closely the three-dimensional structure of the event.

[37] As mentioned above, the space-based observations of the FTEs were accompanied by ground-based radar observations in the conjugate ionospheres, a few minutes delayed to the Cluster observations. Figure 4 (sixth panel) presents the average LOS Doppler velocities of the Finland radar beam 3 and Syowa East radar beam 0 averaged over the low magnetic latitudes of $\sim 74.5^\circ - 76.0^\circ$N and $\sim 74.5^\circ - 76.0^\circ$S, respectively. These magnetic latitudes correspond to the magnetic Cluster 1 footprints shown in Figure 2 and to the counterparts in the Southern Hemisphere. As discussed in detail by *Wild et al.* [2001, 2003] the averaged LOS Doppler velocities show a characteristic pulsing at the time of the observed FTEs. Typically flows peaked 1–2 min after the "center" time of the FTE observations made by the Cluster spacecraft. These 1–2 min delays are expected due to the propagation of the plasma particles down the magnetic field lines. Indeed, given the delayed response of the ionosphere, Wild and coworkers suggested that a one-to-one correlation between the in situ and ionospheric signatures of FTEs should not be expected. However, the observed Doppler velocities indicate a plasma flow away from the radar in a westward direction for the Finland radar and eastward for the Syowa radar. These flow patterns are consistent with the expected motion of newly formed magnetic flux tubes connected to the Northern and Southern Hemisphere, respectively. The open flux tubes connected to the Northern Hemisphere are dragged dawnward and poleward and the counterparts connected to the Southern Hemisphere are dragged duskward and poleward due to magnetic tension and the antisunward motion of the solar wind.

[38] In order to put the localized observations of the Finland radar in a global context, we shall employ the "map potential" technique developed by *Ruohoniemi and Baker* [1998] to produce global convection maps of the Northern Hemisphere. We shall only concentrate on the Northern Hemisphere here in order to link the mesoscale ground-based observations to the Cluster observations utilizing the Cluster magnetic footprint obtained from the MHD model as reference. The "map potential" technique combines LOS velocities of multiple radar stations via a spherical harmonic fitting algorithm on a polar grid. At grid points were no radar data is available the statistical model of *Ruohoniemi and Greenwald* [1996], parameterized by IMF conditions, is used to stabilize the solution.

[39] Figure 5 (left) presents dayside Northern Hemisphere ionospheric convection maps; each averaged over 5 min at the center times of the FTE observations. Overlaid on the convection maps are the averaged (also over 5 min) open-closed field line boundaries (OCFLBs) obtained from the MHD run indicated by the white/black dashed lines and the Cluster magnetic footprint for the times of the observed FTEs (compare Figure 2) indicated as the white/black dots. The instantaneous Cluster footprints were obtained using streamline calculations exploiting the Cluster 1 (Rumba) orbit location at the times of interest and the three-dimensional MHD data. Furthermore the FOV of the Finland radar is indicated as reference for the observations presented in Figure 4.

[40] Since the convection maps are produced by averaging the data over 5 min to compensate for limited LOS data, short velocity fluctuations as presented in the Finland beam 3 (see Figure 4, sixth panel) are smoothed out. The convection maps are not intended to accurately represent small-scale features; instead they provide an estimate of the general ionospheric convection pattern and the "bottom" layer of the "point-to-point" mapping as shown in Figure 6. Superimposed on these patterns are the small-scale flow disturbances due to the individual FTEs.

[41] The gray scale-coded dots in Figure 5 (left) indicate locations where radar data are available. The vectors drawn from these dots show the resultant vector of the LOS velocity measurement at that location and the fitted flow velocity component normal to the LOS direction at the same location. Dots and vectors are gray scale coded in accordance to the velocity magnitude, as indicated by the gray scale on the left-hand side. It is worth noting that in regions where radar data are unavailable, the ionospheric convection flow estimate is only based upon the statistical patterns shown in the work of *Ruohoniemi and Greenwald* [1996]. In these regions, care should be taken in the interpretation of the "map-potential" solution (we shall return to this fact later in the modeling section).

[42] As shown only limited radar data are available and mainly localized dawnward and at lower latitudes than the Cluster footprint. Owing to the insufficient radar data available, the general convection patterns shall be shown here only for completeness but shall not be used for comparisons since they are mainly based upon the statistical patterns and do not incorporate the fluctuation due to the

FTEs. This is especially evident comparing the convection patterns of 0954 UT with 1045 UT, since under similar IMF conditions but with more radar data available the throat region shifts by over one hour of MLT in duskward direction.

[43] The convection maps in Figure 5 (left) show that for the times of the FTEs the ionospheric flows in the prenoon

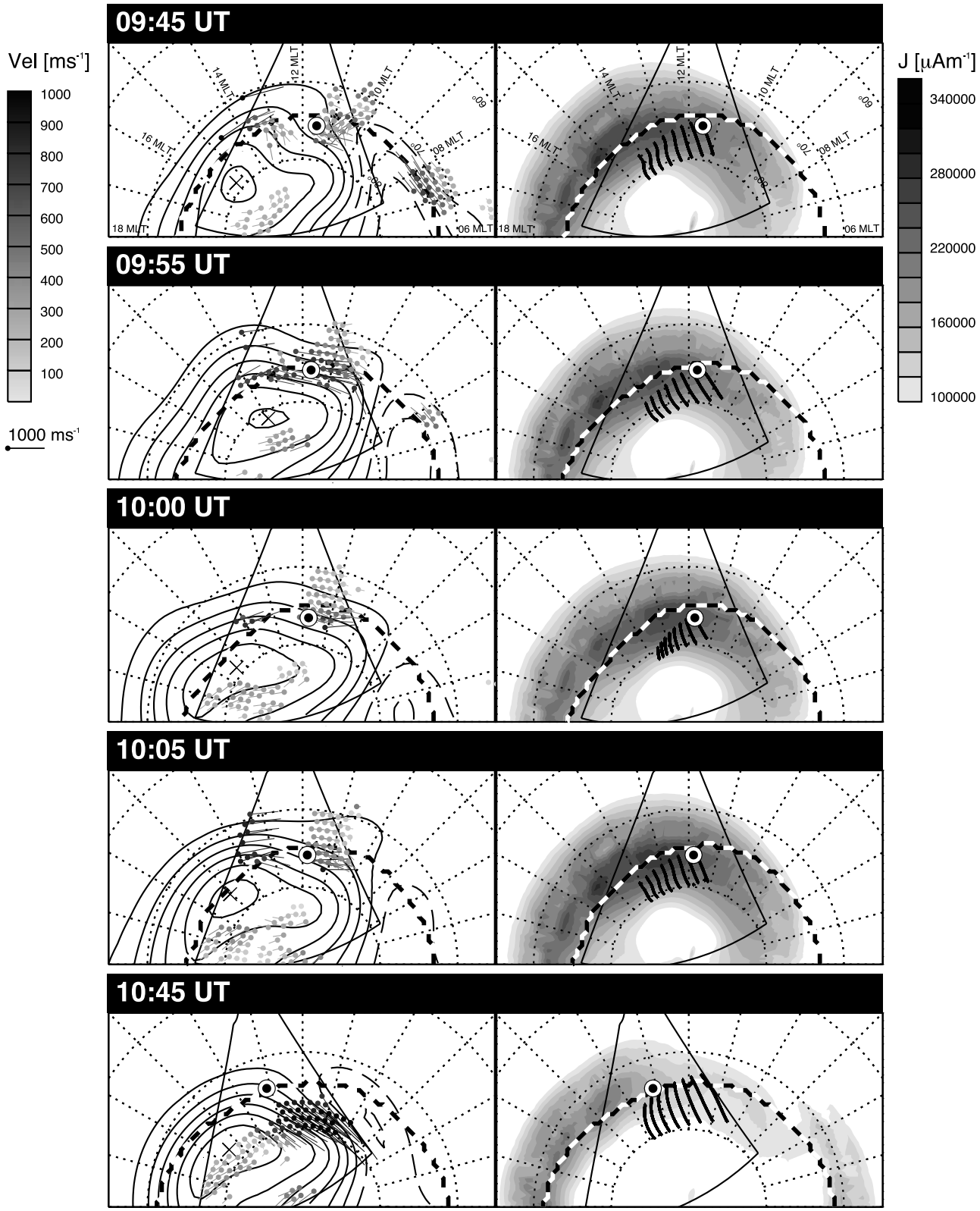

Figure 5

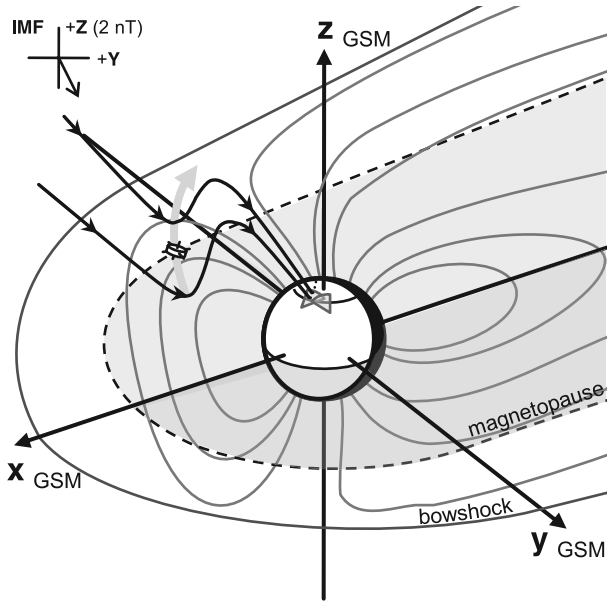

Figure 6. Schematic indicating the idealized magnetic field topology after reconnection has taken place. The solid black lines indicate a magnetic field line after reconnection took place in two time steps. The motion of this field line is associated with plasma and field perturbations which can be seen by the Cluster spacecraft (the location of the Cluster tetrahedron is indicated by the spacecraft symbol). The black arrows indicate the plasma propagation along the newly reconnected magnetic field line down to the ionosphere. The footprint motion can then be seen in the FOVs of the SuperDARN radars indicated as light gray shapes on the ground and can be pinpointed using several SuperDARN radars.

to postnoon sector from ~10–18 MLT and between 70°–80°N MLAT were predominantly westward, with ionospheric plasma moving from later MLTs to earlier ones and turning poleward as indicated in the western and middle portion of the Finland radar FOV with flow speeds exceeding 1000 ms^{-1}.

[44] Despite the limited backscatter in the Northern Hemisphere ionosphere, the flows in regions where radar data are available show a general consistency with inferences regarding the motion of flux tube footprints in terms of their location [*Crooker and Siscoe*, 1990; *Toffoletto et al.*, 1990] and theoretical predictions of expected flow patterns [*Cowley and Lockwood*, 1992]. We shall return to the localization of the flow patterns and their associated flux tube footprint motion later in the modeling section.

[45] The LOS velocity features discussed are especially prominent dawnward of the location of the Cluster 1 magnetic footprint, here the radar data clearly indicate a westward and poleward motion of the ionospheric plasma. *Wild et al.* [2003] performed a comparison of the Northern and Southern Hemisphere for the times of interest. The analyses of the Southern Hemisphere ionospheric convection maps showed exclusively eastward and poleward flows between 75°–80°S MLAT with ionospheric plasma moving from earlier to later MLTs. *Wild et al.* [2003] concluded from the convection map comparison that the observed ionospheric flow patterns in the prenoon and postnoon sector must have been caused by the motion of newly opened flux tubes produced by either an X-line extending over several hours of local time (at least 4 h) or multiple reconnection sites separated in azimuth by a similar displacement.

[46] The simultaneous Cluster and SuperDARN radar observations can be schematically summarized in Figure 6 (assuming a reconnection site located equatorward of the Cluster spacecraft). The Cluster in situ measurements of the magnetic field and the plasma perturbations caused by the newly opened flux tube motion form the "top layer" of the point-to-point mapping, and the SuperDARN radar observations represent the conjugate ionospheric responses of the flux tube footprint motion forming the "bottom layer."

[47] Following reconnection on the dayside magnetopause (as schematically indicated in Figure 6), the newly opened flux tubes are dragged over the magnetopause due to the combination of magnetic field tension and the antisunward motion of the solar wind (the motion is indicated by the light gray arrow in Figure 6), the resulting plasma and field perturbations can be seen in the Cluster 1 in situ observations (see Figure 4). The flux tubes whose footprints are connected to the Northern Hemisphere can be tracked by the SuperDARN radars by observing electron irregularities in the conjugate ionosphere which are $\mathbf{E} \times \mathbf{B}$ drifting with the newly opened flux tubes. These perturbations are manifested as westward and poleward plasma flows. We shall return to this "top-bottom"-layer view later in the modeling section.

[48] To place the localized Cluster and SuperDARN observations into a global context as indicated in Figure 6, it is necessary to perform a global simulation of the geospace environment focusing on (1) the global field line topology of the FTE flux tubes, (2) determination of the location of the reconnection X-line/s, (3) the evolution of

Figure 5. (left) The streamlines and vectors of the ionospheric flows derived from the SuperDARN velocity measurements in the dayside Northern Hemisphere and obtained from the "map potential" technique described by *Ruohoniemi and Baker* [1998] averaged over 5 min at the times of the FTEs. The velocity flow vectors are scaled and gray scale coded to indicate flow speeds as described in the key to the left. (right) The electric current density J of the ionosphere at 100 km altitude extracted from the Ridley ionosphere model included in the BATS-R-US MHD run for the predominant times of the observed FTEs. The electric current density is scaled as indicated in the key to the right. Overlaid are the field line traces of the FTE motion obtained from the Cooling–BATS-R-US mapping indicated by the solid black lines. Overlaid in all plots is a magnetic local time grid, the FOV of the Finland radar and the OCFLB (white/black dashed line; averaged position over the 5 min) obtained from the BATS-R-US model run as well as the magnetic footprint of Cluster 1 (instantaneous for the times of the FTEs) indicated by the white/black dot.

FTEs and their location in respect to the Cluster spacecraft, and (4) determination of the footprint motion of the newly opened flux tubes in the conjugate ionospheres.

4. Models

[49] By employing a global MHD simulation in combination with space- and ground-based observations, it is possible to estimate the large-scale spatial characteristics of the observed FTEs (within the boundaries of the modeling precision). In order to study also the temporal evolution, we have employed a realistic flux tube motion model based on that of *Cooling et al.* [2001] (subsequently referred to as the "Cooling model"). Utilizing these models we are able to track the motion of the newly opened flux tubes across the magnetopause and, based on this information, we are able to model the three-dimensional topology of the magnetic field at the times of the FTEs.

[50] The correlation of the models and the measurements was undertaken by using VisAn MHD (http://www.visan.net.ms) [*Daum*, 2007] which allowed a direct analysis and visualization of the correlations. VisAn MHD is a Matlab toolbox developed at Lancaster University, it is designed to provide users with an easy to use analysis and visualization tool for the various numerical models available to the community. VisAn MHD follows the first generation of standardized software tools (cf. CISM-DX) [*Wiltberger et al.*, 2005, and references therein] which allows users to employ various sophisticated numerical models in their studies by using standardized widely known syntax structures. This feature allows these tools to be widely used in different communities. VisAn MHD is released under the GNU General Public license (GNU GPL) and freely available to the different research communities.

4.1. Global MHD Model (BATS-R-US)

[51] In this study we use the BATS-R-US MHD code [*Powell et al.*, 1999] which was originally developed by the Computational MHD Group at the University of Michigan, now Center for Space Environment Modeling (CSEM: http://csem.engin.umich.edu). The code used in this study is version 7.73 which is part of the Space Weather Modeling Framework (SWMF) described by *Tóth et al.* [2005]. The BATS-R-US code solves three-dimensional MHD equations in a finite volume form using numerical methods related to Roe's Approximate Riemann Solver [*Roe*, 1981]. The code therefore utilizes an adaptive grid composed of rectangular blocks arranged in varying degrees of spatial refinement levels. A detailed description of the model and the numerical/parallel implementation can be found in the work of *Gombosi et al.* [2003].

[52] The BATS-R-US code executed within the SWMF is coupled with the Rice Convection Model (RCM) which represents the inner and middle magnetosphere with coupling to the ionosphere [*Toffoletto et al.*, 2003]. The RCM represents the particles in terms of multiple fluids. Its equations and numerical methods have been specifically designed for an accurate treatment of the inner magnetosphere, including the flow of electric currents along magnetic field lines to and from the conducting ionosphere. The RCM computes these currents and the associated electric fields self-consistently. It assumes perfectly conducting field lines and employs a precomputed time-dependent magnetic field with associated induction electric fields. The Vasyliunas equation [*Vasyliunas*, 1970] is used to compute the magnetic-field-aligned currents (Birkeland currents), and Ohm's law is used to compute the self-consistent ionospheric potential distribution. A detailed description of the BATS-R-US/RCM coupling can be found in the work of *De Zeeuw et al.* [2004].

[53] The model employed here is the BATS-R-US model included in the SWMF version 2. Initial runs have been performed at the Community Coordinated Modeling Center (CCMC) at NASA Goddard Space Flight Center (GSFC); runs under the SWMF version 2.3 have been recently performed on the Lancaster High Performance Cluster and showed equivalent results. In both sets of runs we have halved the observed solar wind density to obtain reasonable magnetopause locations, consistent with the in situ measurements from Cluster. The model runs were executed with a 0.25 R_E ($\sim$1600 km) resolution in the near-tail and dayside magnetopause region and a 0.0625 R_E ($\sim$400 km) resolution in the cusp region close to the Cluster position (cf. Figure 2). The adaptive nonuniform numerical grid was then interpolated onto an uniform regular cartesian grid with a resolution of 0.1 R_E ($\sim$640 km) inside a bounding box of -30 to 15 R_E in the **x** direction and ± 15 R_E in the **y** and **z** directions, respectively. The simulation was implemented with real time-dependent upstream inflow conditions obtained from the instruments on board the ACE satellite (cf. Figure 3). The magnetic equatorial strength of the Earth's dipole field was set to $-31{,}100$ nT (default for the SWMF in the predefined $|PLANET|$ command), while the orientation of the magnetic field was updated in real time.

[54] The ionospheric conduction model included in the SWMF run is the Ridley ionosphere model based on the work of *Ridley and Liemohn* [2002] and *Ridley et al.* [2004]. It is a two-dimensional electrostatic potential solver that obtains the field-aligned currents from the global magnetosphere (GM) module included in the SWMF and employs a statistical auroral ionosphere conductance model driven by the solar irradiation index (F10.7) and by the field-aligned current patterns. From the different models included in the SWMF it is possible to retrieve a wide range of output parameters from the different regions of interest. The model outputs include the plasma parameters (atomic mass unit density n; kinetic pressure p; velocity v_x, v_y, v_z), the magnetic field components B_x, B_y, B_z, and the electric current components j_x, j_y, j_z. As a byproduct of the RCM-Ridley coupling the ionospheric electrodynamic parameters (electric potential Φ; Hall and Pedersen conductance Σ_H, Σ_P) and the ionospheric electric current density J can be obtained. The wide range of parameters allows us to model the features of the FTEs on a global scale without the limitations and boundary restrictions of an empirical model.

4.2. Open Flux Tube Motion Model (Cooling Model)

[55] In order to be able to study the temporal evolution of the FTEs we employ the Cooling model [*Cooling et al.*, 2001]. While a detailed description of this model is not appropriate here, we shall outline the basic elements of the simple implementation used in this study. The Cooling model itself is an evolution of the model by *Cowley and*

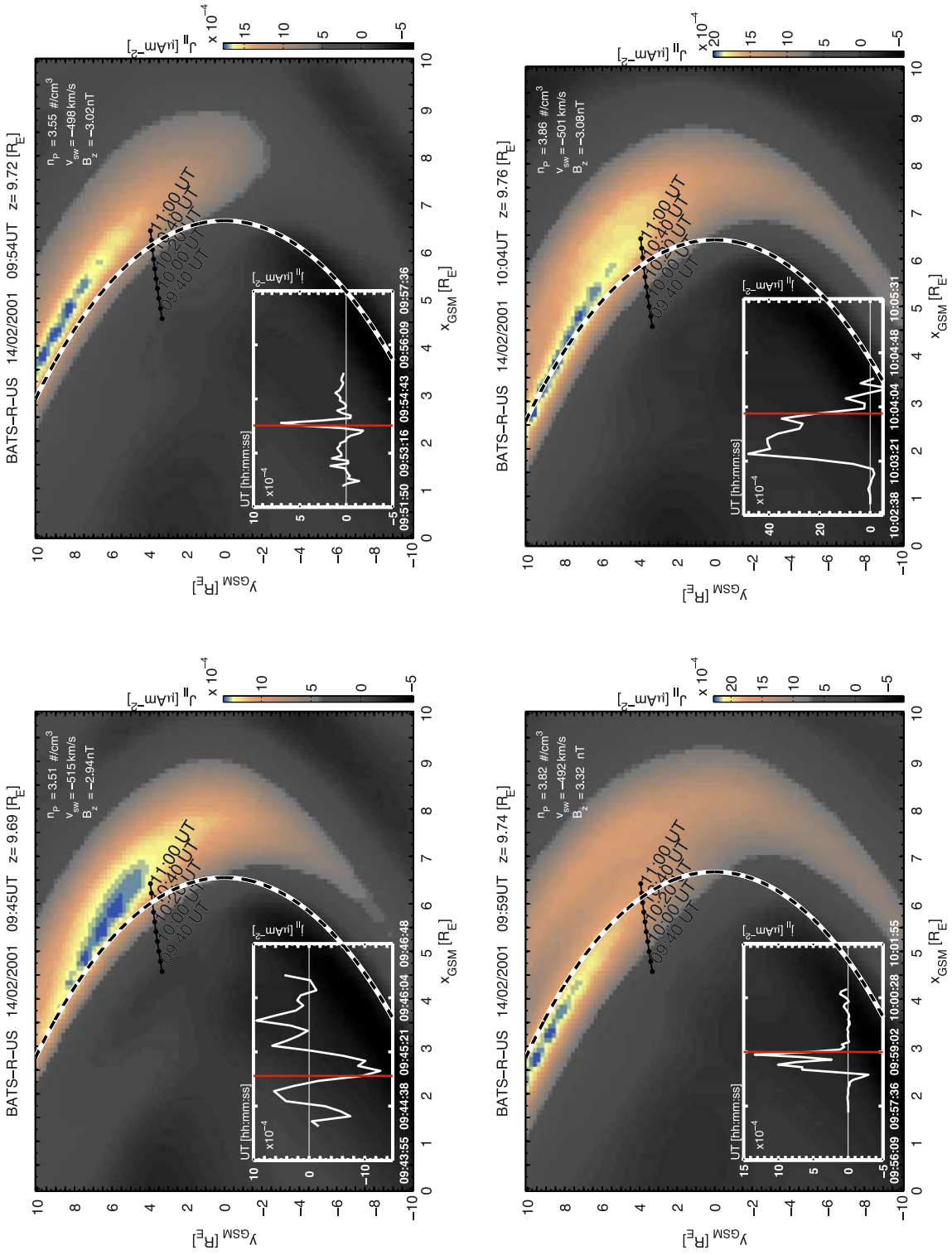

Figure 7. The field-aligned current density in the GSM **y**−**z**-plane at the z position of Cluster 1, for the times of the magnetospheric FTEs (see Figure 4; 0945 UT, 0954 UT, 0959 UT, 1004 UT). The electric current density is color coded as indicated in the keys to the right of each frame. Overlaid on each frame is the Cluster 1 orbit projection in the corresponding reference frame. The white/black dashed lines indicate the inner magnetopause boundary after *Shue et al.* [1997] parameterized by the IMF parameters shown in the upper right-hand corner of each frame. The insets of each frame show the field-aligned electric current densities obtained from the curlometer technique [*Dunlop et al.*, 1988] exploiting the FGM data from all four spacecraft at 4 s resolution.

Owen [1989], it considers the draping and strength of the magnetosheath magnetic field, the magnetosheath flow velocity, and the density over the surface of a simple parabolic magnetopause [*Kobel and Flückiger*, 1994; *Spreiter et al.*, 1966] in order to evaluate the velocity of the point where the newly reconnected flux tubes thread the modeled magnetopause. This calculated instantaneous velocity is the velocity of the rest frame of a reconnected field line, the so-called de Hoffmann-Teller frame [*De Hoffmann and Teller*, 1950], in which the electric field transforms to zero. On the basis of this rest frame velocity and the simple linear relationship between the magnetosheath velocity, the magnetic field direction and the Alfvén speed derived by *Cowley and Owen* [1989], the Cooling model calculates the de Hoffmann-Teller velocities of the flux tubes connected to the Northern and Southern Hemisphere, respectively.

[56] From these velocities, the motion of the points at which the open magnetic flux tubes thread the magnetopause can be traced via iteration over the surface of the dayside magnetopause from any location on the surface of the magnetopause. In the applied model, we are therefore able to monitor the subsequent motion of the newly reconnected flux tubes (i.e., FTEs) away from the defined X-line (characterized by the locus of 180° shear).

[57] This allows us to use the simple Cooling model calculations (i.e., the computed points tracing the motion of open flux tubes across the surface of the magnetopause) as start points for field line traces using the fully three-dimensional MHD simulation data. The MHD ''snapshots'' of the magnetic field line topology following reconnection are then used to ascertain the structure and evolution of the observed FTEs.

[58] This combination of a global model and a motion model allows us to get a deeper insight into the global dynamics especially since the Cooling model was used in previous observational studies to characterize the large-scale motion of FTEs in combination with space- and ground-based observations [e.g., *Dunlop et al.*, 2005; *Wild et al.*, 2005, 2007] we are confident in the combination of the two models as described further down. Also the combination represents a further validation method for the MHD model comparison.

5. Model Results

[59] The simultaneous observations of FTE signatures by the space- and ground-based instruments discussed above shall now be put into a global context using the BATS-R-US MHD code in combination with the Cooling model. The presented combination analysis technique was first presented by *Daum and Wild* [2006] and a similar approach will be employed here.

[60] We shall first consider particular observational features and compare them to the modeled results before we put the individual comparisons in a global context. First, we shall consider the location of the reconnection site(s) on the dayside magnetopause in the model. *Wild et al.* [2003] pointed out that a decision between either an X-line extending over many hours of local time (at least 4 h) or multiple reconnection sites separated in azimuth by a similar displacement is difficult to make based on the observations alone. In order to revisit this uncertainty, we have simulated the predominant time of interest from 0930 to 1100 UT on the 14 February 2001 using the BATS-R-US global MHD code. The inflow boundary conditions for the run are shown in Figure 3 and the model was computed with a grid resolution as described above.

[61] In order to identify the probable location and spatial dimension of the reconnection site(s) responsible for the observed FTE signatures we shall first investigate the field-aligned currents ($j_{\|}$) adjacent to the magnetopause. As indicated by *Crooker and Siscoe* [1990], Russell and Elphic type FTEs and their associated reconnection sites can be identified as patches of open field lines on an otherwise closed magnetopause. These ''holes'' in the Chapman-Ferraro magnetopause, and the associated current systems which emanate from these ''holes,'' result in an increased electric current density parallel to the magnetic field. Since these ''holes'' are a feature of the reconnection process involved in the forming of FTEs, the conclusion made by *Crooker and Siscoe* [1990] can also be widened to non Russell and Elphic type FTE models. Therefore, in the simulations, we can associate enhanced current density patches with magnetic reconnection sites at the magnetopause.

[62] Figure 7 shows the modeled field-aligned current density in the GSM $\mathbf{x}-\mathbf{y}$ plane at the z position of Cluster 1. To aid the eye, model magnetopause boundaries after *Shue et al.* [1997] are overlaid on the projections, indicated by the white/black dashed lines and parameterized by the solar wind conditions as indicated in the upper right hand corner of each frame. Here it should be mentioned, that the magnetopause boundary after *Shue et al.* [1997] is only shown as an indicator for the boundary and not to accurately describe the MHD model boundary.

[63] The current sheet slices show well-defined patches of increased electric current density of $10-20 \times 10^{-4}$ $\mu\mathrm{Am}^{-2}$ in an area of $4 < x < 7$ and $4 < y < 8$ R_E adjacent to the modeled [*Shue et al.*, 1997] magnetopause. These patches correspond to the reconnection processes indicated by the observations. In the simulation these patches propagate in antisunward direction around the magnetopause. It can be seen for further time steps in the MHD simulation, that the patches (identified by the field-aligned current strength) have moved downtail along the magnetopause by several Earth radii and that the field-aligned current strength at the former x, y location has decreased. Owing to the 1-min resolution of the MHD simulation these patches (at the former x, y location as shown in Figure 7) disappear after one to three ''snapshots'' after the FTE observations. This corresponds to the time frames given by *Penz et al.* [2007] of reconnection bursts lasting about 2.6 ± 0.9 min.

[64] The insets of Figure 7 show the field-aligned electric current density at 4 s resolution exploiting FGM data from all four spacecraft using the so-called curlometer technique [*Dunlop et al.*, 1988]. The field-aligned current densities show that at the ''center'' times of the FTEs a defined structure is passing over the position of Cluster which can be identified by the peaks lasting about 30 s. From the full resolution FGM data at 64 vectors/s it can be inferred that these structures are passing over the spacecraft formation with a velocity of approximately 96 km/s. In comparison with the electric current density slices from the MHD model

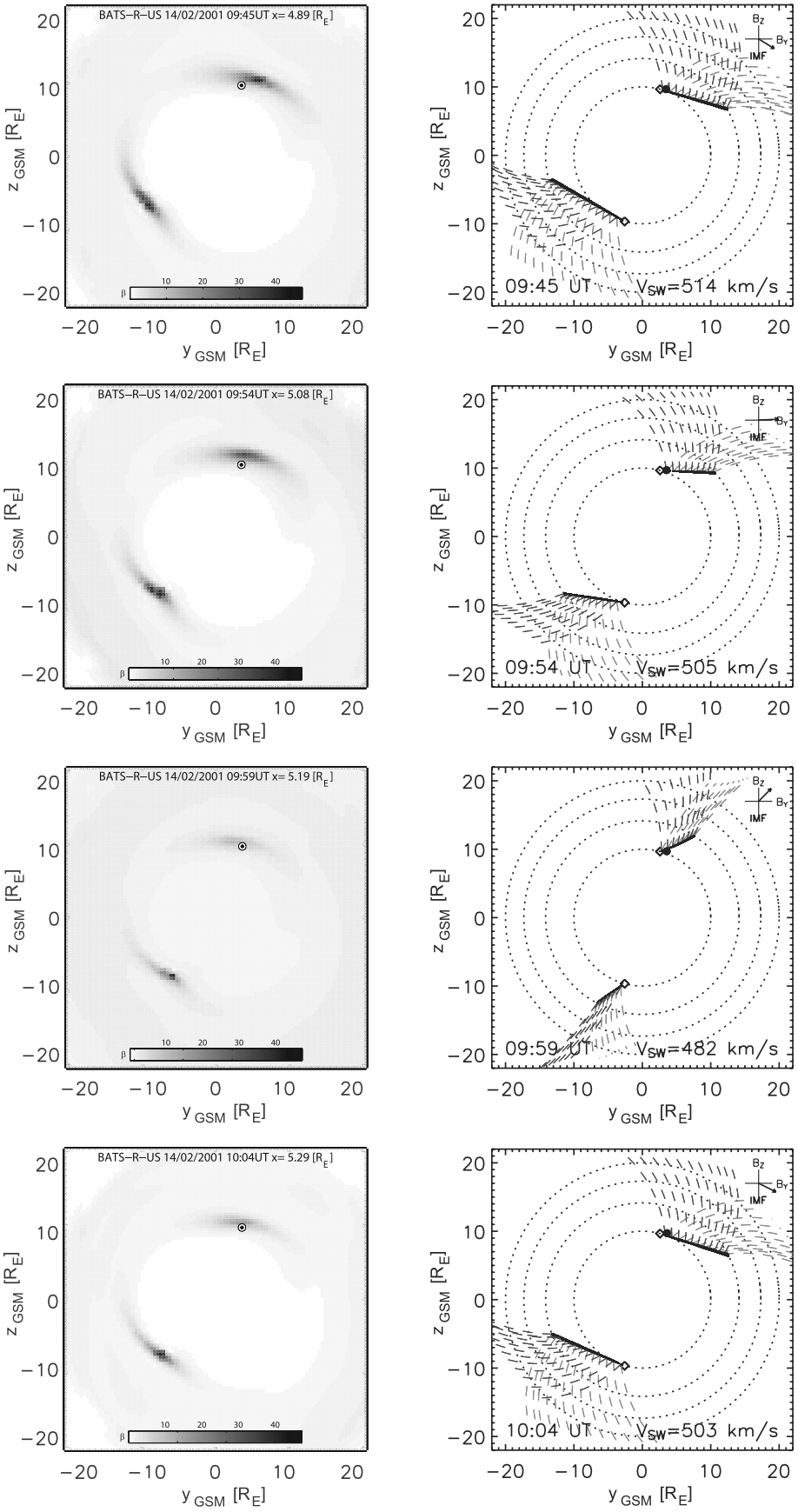
BATS–R–US 14/02/2001 09:45UT x= 4.89 [R_E]
09:45 UT V_SW=514 km/s
BATS–R–US 14/02/2001 09:54UT x= 5.08 [R_E]
09:54 UT V_SW=505 km/s
BATS–R–US 14/02/2001 09:59UT x= 5.19 [R_E]
09:59 UT V_SW=482 km/s
BATS–R–US 14/02/2001 10:04UT x= 5.29 [R_E]
10:04 UT V_SW=503 km/s
z GSM [R_E]
y GSM [R_E]
β
B_z
B_y
IMF

Figure 8

these values show a good correlation. The time of the MHD model slice is thereby indicated by the vertical red line in the insets. Owing to the 1-min resolution in the MHD model these short-time fluctuations can not be reproduced.

[65] Assuming that $j_{\|}$ enhancements at the magnetopause are a proxy for reconnection, we can conclude from the model results that the reconnection site/s seen in the simulation data are localized at the postnoon sector of the magnetopause and extend over at least ~3.5 h MLT in close vicinity of the modeled magnetopause in a narrow band of 1 R_E (for the GSM $\mathbf{x}-\mathbf{y}$ plane at the z position of Cluster 1; see Figure 7). The MHD model therefore shows a bias toward an antiparallel merging scheme as described by *Crooker* [1979] and *Luhmann et al.* [1984]. This bias is often seen in MHD simulations [e.g., *Ogino et al.*, 1986; *Berchem et al.*, 1995; *Fedder et al.*, 2002; *Park et al.*, 2006] especially with a strong $B_y \gg 0$ component of the IMF and a nonzero dipole tilt present.

[66] The modeled results shown in Figure 7 also agree with the studies undertaken by *Penz et al.* [2006a, 2007] which reported that the reconnection processes responsible for the FTEs were located at a distance of ~1.4 R_E (normal) along the magnetopause from the Cluster spacecraft position. The enhanced field-aligned current patches in Figure 7 show a close correlation with these predicted distances.

[67] To ascertain further whether antiparallel merging [*Crooker*, 1979; *Luhmann et al.*, 1984] or component merging [*Sonnerup*, 1970, 1974; *Cowley*, 1973, 1976; *Gonzales and Mozer*, 1974] is predicted by the MHD model, we have derived the plasma beta parameter ($\beta = p/(|B|^2/2\mu_0)$) in the GSM $\mathbf{y}-\mathbf{z}$-plane at the x-location of Cluster for the times of the magnetospheric FTEs, see Figure 8 (left). A highly structured plasma beta component in the models high-latitude magnetopause region would suggest anti-parallel merging as indicated by *Fedder et al.* [2002] and *Berchem et al.* [2008].

[68] In Figure 8 (left) it can be seen, that two regions of high plasma beta ($\beta \gg 10$) can be clearly distinguished in the Northern and Southern Hemisphere. Following the description in the work of *Berchem et al.* [2008] the MHD model predicts antiparallel merging with two reconnection sites with a comparable azimuth displacement in the Northern and Southern Hemisphere, respectively. This would also agree with a recent modeling study undertaken by *Park et al.* [2006]. This study showed that under $B_z < 0$ and $B_y > 0$ IMF conditions, and a nonzero dipole tilt, antiparallel merging in the high latitudes is dominant over component merging. As shown by recent observational studies [e.g., *Sandholt et al.*, 2004; *Massetti*, 2006; *Trattner et al.*, 2006], such a clear characterization cannot be seen in the observations. Observations of the magnetosphere in combination with the conjugate ionospheres led these authors to conclude that it is most likely that the signatures observed are actuated by a "mixed" reconnection topology, resulting from a superposition of antiparallel reconnection at high latitudes and component merging in the subsolar regions. Also it is worth noting that the presented ground- and space-based observations do not favor either of the merging concepts.

[69] Following *Park et al.* [2006] characterizations and the indications given by the plasma beta parameter derived from the model, we follow the antiparallel merging topology for the further analysis. Nevertheless it should be mentioned here that the antiparallel merging topology as indicated by the MHD model run is dependent upon the resistivity model used in the simulation as outlined recently by *Berchem and Richard* [2007]. *Berchem and Richard* [2007] stated that the merging line grows with resistivity. Therefore it could be that no component merging is seen in the presented simulation due to insufficient resistivity. Since neither the observations nor the models favor either the antiparallel nor component merging description, we follow the characterization of *Park et al.* [2006] in favor of antiparallel merging.

[70] The next step of the analysis is to evaluate the evolution of the flux tubes opened at the reconnection sites and the general field line topology. Consequently, we have employed the Cooling model to study the motion and large-scale structure of the newly reconnected field lines. The Cooling model considers pairs of open reconnected field lines which are initiated along a model reconnection site (locus of 180° shear). The Cooling model only considers the FTE motion due to the $\mathbf{j} \times \mathbf{B}$ force and the magnetosheath flow, therefore each of the pairs of reconnected field lines can be treated as individual points of reconnection. In order to make the MHD model and the Cooling model comparable, we have modified the Cooling model's magnetopause standoff distance to coincide with that of the MHD model. Owing to the Cluster in situ observations shown in Figure 4 and the discussions about the northern cusp location in the work of *Wild et al.* [2001, 2003] and *Wilken et al.* [2001], we have also modified the location of the cusp singularities in the Cooling model. Usually, the cusps are located on the magnetopause surface, at GSM $y = 0$ and an x position midway between the magnetopause nose standoff distance and $x = 0$. In this case, we have simply rotated the line

Figure 8. The plasma beta parameter derived from (left) the BATS-R-US model runs and (right) the Cooling model runs for an antiparallel merging topology [*Crooker*, 1979; *Luhmann et al.*, 1984]. Both simulation results are projected into the GSM $\mathbf{y}-\mathbf{z}$-plane, looking earthward from the Sun. BATS-R-US model (Figure 8, left): contour plots of the plasma beta parameter derived from the BATS-R-US simulation data at the x position of Cluster 1. The data are gray scale coded in accordance with the key to the bottom of each frame. The white/black dots mark the Cluster 1 position as reference to the Cooling model. Cooling model (Figure 8, right): the IMF clock angle used for each computation is indicated in the small insets of each frame. The solid black lines represent the merging lines from which pairs of reconnected flux tubes are initiated. The trace of these pairs over the magnetopause are presented with the dashed lines, the dark gray dashed lines represent flux tubes connected to the Northern Hemisphere, and the light gray dashed lines represent flux tubes connected to the Southern Hemisphere. The concentric dotted circles represent the radius of the modeled magnetopause at 5 R_E intervals along the $\mathbf{x}$ direction; the cusps are considered to be point singularities marked by the two diamonds. The Cluster 1 position is marked with the black dot.

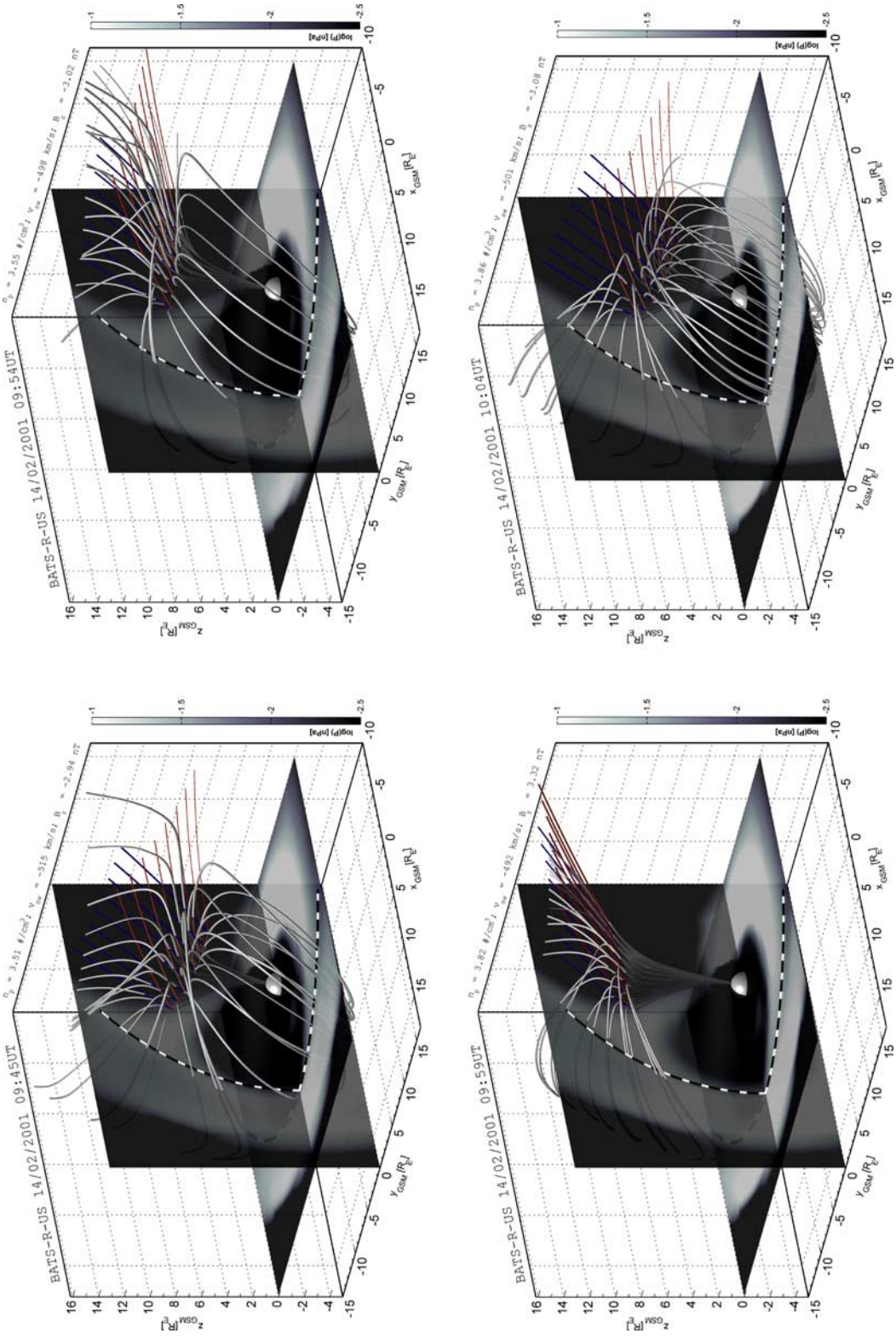

Figure 9. Three-dimensional field line topology for the Cooling flux tube motion traces (compare Figure 8, right) at the times of the FTEs mapped from the high-resolution MHD data. The blue traces (compare Figure 8, dark gray) representing flux tubes connected to the Northern Hemisphere and the red traces (compare Figure 8, light gray) represent traces to the Southern Hemisphere. The two slice planes represent the gray scale-coded logarithmic kinetic pressure as indicated in the key to the right of each frame. The white/black dashed lines indicate the inner magnetopause boundary after *Shue et al.* [1997] parameterized by the IMF parameters shown on the upper *y*-axis of each frame. The light gray lines represent the magnetic field line topology mapped from the Cooling traces.

joining the northern and southern cusps by 15° about the Earth-Sun line (toward positive *y*-vales in the Northern Hemisphere and negative *y*-vales in the Southern Hemisphere) with the result of bringing the Northern Hemisphere cusp closer to the location of the Cluster spacecraft.

[71] Taking this into account and the results of a recent study undertaken by *Fear et al.* [2007] in which the accuracy of the Cooling model was compared with Cluster measurements, we are confident in the overall mapping between the Cooling model traces and the MHD model data to investigate the global structure and evolution of the presented FTEs. It should be noted here that a direct matching between the two models will never be achieved, since the Cooling model only includes a very basic magnetosheath model and no dipole tilt but the study by Fear and coworkers showed that under predominantly southward IMF or a dominant B_y component of the IMF, the FTE velocity predictions matched the Cluster observations reasonably well. The open flux tube traces derived from the Cooling model will therefore provide well-defined starting points for the mapping process between the FTE motion across the high-latitude magnetopause and the conjugate ionosphere exploiting the high-resolution MHD data.

[72] Figure 8 (right) shows the results of the Cooling model runs for an antiparallel merging line in the high-latitude magnetopause in close vicinity to the Cluster formation as well as the counterpart merging line in the Southern Hemisphere. The results shown in Figure 8 are projected onto the GSM **y**−**z**-plane looking earthward from the Sun. The concentric dashed circles indicate the shape of the modeled magnetopause in 5 R_E intervals along the **x** direction. The IMF clock angle for the simulation runs are shown in the insets in the upper right-hand corner of each frame. The solar wind speed used as an input to the model is taken from the ACE solar wind observations shown in Figure 3.

[73] The position of Cluster is marked as a black dot in the high-latitude postnoon sector at $x \sim 5.5\ R_E$, $y \sim 3.5\ R_E$, and $z \sim 9.8\ R_E$. The solid black lines indicate the most likely X-line locations derived from the magnetic shears (locus of 180° shear) and the corresponding magnetopause currents. As noted above, the X-line/s should be seen as the general locations of the multiple reconnection sites from which the FTEs emerged. The Cooling model assumes the cusps to be point singularities, the locations are marked by the diamonds. The dashed lines originating from the merging line/s represent the pairs of open reconnected flux tubes connected to the Northern (dark gray) and Southern (light gray) Hemispheres, respectively. We note that in this case, all newly opened flux tubes move antisunward. As such, at the Northern Hemisphere X-line newly opened flux tubes connected to the Southern Hemisphere are dragged poleward and tailward across the X-line, suggesting that steady reconnection at this location is impossible [*Cowley and Owen*, 1989; *Cooling et al.*, 2001]. The same is true at the X-line in the vicinity of the southern cusp.

[74] Concentrating on the flux tubes connected to the Northern Hemisphere (cf. Figure 8 (right); dark gray dashed lines) at the position of the Cluster spacecraft, the general motion can be identified as predominantly poleward and somewhat dawnward along the magnetopause. This motion results from the antisunward motion of the solar wind and the $\mathbf{j} \times \mathbf{B}$ magnetic tension force acting upon the curved, newly reconnected field lines. The expected motion of these flux tube footprints in the conjugate Northern Hemisphere ionosphere is therefore expected to be westward and poleward. *Wild et al.* [2001, 2003] have shown comparable motions seen in the flow patterns of the SuperDARN radar systems (see Figure 5, left).

[75] On the basis of the open flux tube traces provided by the Cooling model in the Northern Hemisphere, we have computed the three-dimensional point-to-point mappings between the flux tube traces and the conjugate ionosphere at an altitude of 100 km (see Figure 9) exploiting the three-dimensional magnetic field data of the MHD simulation to perform the streamline tracing calculations. Figure 9 presents the large-scale three-dimensional magnetic field line topology of this Cooling-BATS-R-US mapping process at the times of the FTEs. The light gray lines represent MHD-derived magnetic field lines that pass through the traces given by the Cooling model. The traces are indicated by the blue (connected to the Northern Hemisphere) and red lines (connected to the Southern Hemisphere). The contour slices represent the logarithmic kinetic pressure of the MHD model on the uniform regular cartesian grid with a resolution of 0.1 R_E (∼640 km) gray scale coded in accordance with the key to the right of each frame. Overlaid in the GSM **x**−**y** and GSM **x**−**z**-plane are the inner magnetopause boundaries after *Shue et al.* [1997] parameterized with the parameters to the top of each frame (cf. parameters Figure 7).

[76] The field topologies exhibit a clearly open-closed field line structure. The field lines in close proximity to the Cluster location ($x \sim 5.3\ R_E$, $y \sim 3.6\ R_E$, and $z \sim 9.8\ R_E$; cf. Figure 8) reveal an L-shaped curved structure. The comparison of Figures 7 (field-aligned currents), 8 (Cooling traces), and 9 (3-D Cooling-BATS-R-US mapping) reveals that the field lines at higher latitudes above the reconnection sites ($z > 10\ R_E$; reconnection sites are indicated in Figure 7, they are slightly higher than the ones given by the Cooling computations) have an open field line topology with their direction mainly influenced by the clock angle of the IMF. The field lines at lower latitudes than the reconnection sites ($z < 10\ R_E$) show a closed field line topology but are deformed and stretched toward the points of reconnection. Following the open magnetic field lines from the ionosphere to the high-latitude magnetopause the field lines perform at first a ''right turn'' and then a sharp ''left turn'' toward dawn. After the turns the field lines are stretched around the magnetopause. These magnetic field line perturbations and the associated plasma perturbations correspond to the observation of the FTE features as postulated first by *Russell and Elphic* [1978] and *Dubinin et al.* [1980] and shown in Figure 4. The field line perturbations shown in Figure 9 are closely related to the merging line which is shown in the Cooling computations (cf. Figure 8 (right)).

[77] We note that the FTEs at 0945 UT, 0954 UT, and 1004 UT emanated from reconnection sites which occurred under similar negative clock angles (cf. Figure 3h), whereas at 0959 UT the clock angle was predominant northward. Studying the field line topologies for the cases of southward IMF more carefully, we notice that the separation of the open and closed field line topology is coincident with the location of the increased patches of parallel electric current densities as shown in Figure 7 but with a slightly higher

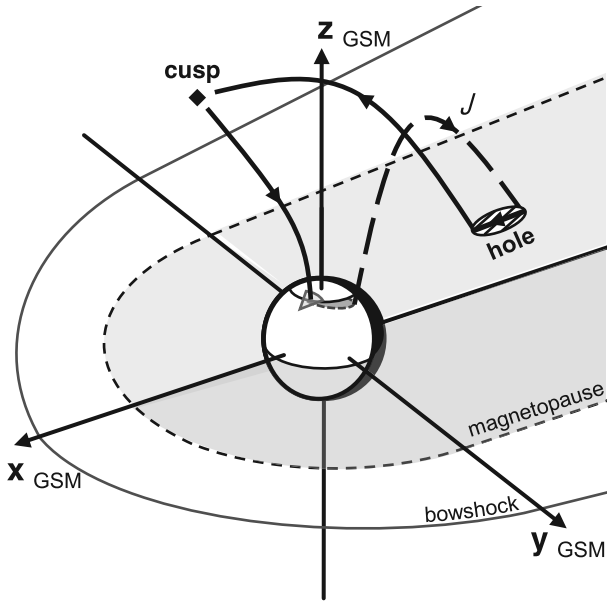

Figure 10. Schematic diagram of the current J associated with the antisunward motion of a newly opened flux tube in a magnetopause hole after *Crooker and Siscoe* [1990]. The solid and dashed lines indicate current flows from the ionospheric footprint to the magnetopause "hole" and back.

offset from the presumable reconnection site ($\sim$0.2–1.0 R_E) than the Cooling merging line. This indicates that at these locations reconnection has taken place and that the "snapshots" in Figure 9 show the newly reconnected field lines in a time instance after reconnection took place.

[78] In contradiction to *Fedder et al.* [2002] the field line topologies and the associated FTEs presented here have caused a localized enhancement of the field-aligned currents as seen in Figure 7. This leads us to believe that the current influences might also be seen in the conjugate ionospheres, as indicated by *Wild et al.* [2001, 2003]. In order to investigate the evolution and influence of the FTE structures in the conjugate ionosphere, we have mapped the magnetic field line topology shown in Figure 9 down to an altitude of 100 km in the Northern Hemisphere ionosphere. The result of the mapping process is shown in Figure 5 (right) as solid black lines on a magnetic local time grid. The traces are overlaid on the Ridley electric current densities obtained from the SWMF Ridley ionosphere module. For comparison to Figure 5 (right) the FOV of the Finland radar, the OCFLB (white/black dashed line) and the Cluster 1 footprint (white/black dot) are overlaid.

[79] Studying the electric current density in Figure 5 (right), we note that in a narrow band between $\sim$72–80°N MLAT enhanced patches of electric current density are evident, generally coaligned with the OCFLB. These patches can be associated with the increased patches of field-aligned currents at the high-latitude magnetopause as presented in Figure 7. The ionospheric currents arise in response to the ionospheric drag on the flux tubes convecting in antisunward direction along the magnetopause. These elongated patches in the ionosphere are the footprints of the magnetopause "holes" associated with the FTEs [*Lundin and Evans*, 1985]. *Crooker and Siscoe* [1990] postulated for Russell and Elphic type FTEs, that the FTEs map as elongated "teardrop" shaped patches into the ionosphere. Furthermore, they showed that the upward current from the elongated end of the footprint flows to the edge of the magnetopause "hole" furthest from the cusp, crosses the hole against the Chapman-Ferraro current, decreases the shielding there, and returns to the ionosphere along the field lines from the near-cusp edge of the "hole"; this is illustrated in Figure 10. As indicated above, the "holes" in the Chapman-Ferro magnetopause are not just characteristic for Russell and Elphic type FTEs and it should be noted here that longer structures passing through the "holes" would most likely also have elongated current responses in the conjugate ionosphere as described in various observational and modeling studies [e.g., *Saunders*, 1989; *Glassmeier and Stellmacher*, 1996; *McWilliams et al.*, 2001; *Pitout and Blelly*, 2003].

[80] Following Crooker and Siscoe's illustration, the several "holes" of the magnetopause presented in Figure 7 are also expected to have elongated footprints in the conjugate ionosphere. These footprints are partially reproduced by the model and can be seen in Figure 5 (right) as elongated patches of enhanced electric current densities in the early afternoon sector as first indicated by *Meng and Lundin* [1986] and *Crooker and Siscoe* [1990] in their observation of auroral arc forms in the Northern Hemisphere. The authors describe these forms as "fan-shaped" arc structures that focus toward the cusp.

[81] We shall further examine the magnetic footprints associated with the location of newly opened flux tubes on the magnetopause that pass in close proximity to the Cluster spacecraft (indicated by solid black lines in Figure 5, right). The footprints in general show a straight path away from the radar covering $\sim$30–60 min MLT from later MLTs to earlier ones following from lower to higher magnetic latitudes. These paths are consistent with the general flow observations made by the SuperDARN radar. This leads us to conclude that the footprints indicate a westward and poleward motion of the newly opened flux tubes across the Northern Hemisphere ionosphere.

[82] As discussed in section 3.2 (Cluster/SuperDARN observations), due to very limited radar measurements, not all of the ionospheric Cooling-BATS-R-US traces are colocated with ionospheric observations. Outside of these regions, the estimated convection pattern should be treated with caution since, due to the lack of measurements, these patterns are only constrained by a statistical convection model parameterized by the general IMF conditions. We shall therefore only concentrate our further comparisons on the times where actual LOS data are available for the areas of the traces, these times are 0945 UT (weak coverage) and 1045 UT (good coverage). Concentrating first on the 09:45 UT convection map (Figure 5, left) the Doppler velocities presented as gray scale coded dots and vectors in the dusk part of the Finland radar at about 1300 MLT show a strong westward (lower magnetic latitudes) and poleward (higher magnetic latitudes) component with velocities of $\sim$1000 ms^{-1}. In the vicinity of the Cluster footprint (where radar data exist and can be compared to the in situ FTE observations), the LOS velocities and convection streamlines are in reasonable agreement with the traces obtained from the Cooling–BATS-R-US mapping. In the higher-latitude region starting from 73°N MLAT the estimat-

ed convection flow is not sufficiently constrained by data to give reasonable results for comparison. The same is true for the 0955 UT, 1000 UT (northward IMF conditions), and 1005 UT maps.

[83] We shall therefore concentrate on the 1045 UT convection map where enough LOS data are available to constrain the convection patterns and to give a substantial base for comparison. Here LOS Doppler velocities presented as gray scale-coded dots and vectors are available over the complete FOV of the Finland radar in a band from 75°–80°N MLAT. In the MLT range from 1100 to 1300 MLT the Doppler velocities exceed $\sim$1000 ms^{-1}. It can further be seen that with enough LOS data present, the throat region of the convection pattern has shifted to 1200 MLT in comparison to 0900–1000 MLT in the other convection maps under similar IMF conditions. Comparing these high velocity LOS data with the Cooling–BATS-R-US traces it has to be noted that they compare well with a minor offset of approximately 10°. This slight offset could be the result from either the MHD simulation in respect to the grid resolution, the Cooling model in respect to the simple models underlying it, or the temporal averaging factor (5 min) for the convection maps. Also another factor, which could lead to the offset, could be the difference between the Cooling magnetopause and the BATS-R-US magnetopause boundary. A slight difference between the locations of the two (cf. Figure 9) would have a stretching/compressing effect on the mapping process. Keeping these factors in mind a slight offset of 10° is acceptable and in terms of modeling (use of two independent models) a good match.

[84] The model results are therefore consistent with the study undertaken by *Wild et al.* [2001, 2003] and extend the former study such that the footprints obtained from the Cooling model and the MHD simulation can explain the ionospheric bursts seen in the radars (see Figure 4, sixth panel) to a good degree and corroborate the one-to-one correlation of the ground- and space-based observations.

[85] Using the technique described above we can now accomplish a general three-dimensional view of the field topology of the FTEs and explain the concurrent observations of the space- and ground-based instruments. We shall finally consider the FTE observation at 1046 UT which had the largest bipolar signature in the B_N component to model the complete set of FTE features discussed above.

[86] The field-aligned currents give an indicator of the probable location and spatial extent of the reconnection site responsible for the FTE observations. Figure 11 (model results) presents the field-aligned currents in the GSM **x**–**y**-plane and in the GSM **y**–**z**-plane as well as the total magnetic field strength. The Cluster 1 location is marked with the white/black dot. We note that the reconnection site has a similar extent as discussed above for the FTEs observed inside the magnetopause (cf. Figure 7). The patchy enhancements of the field-aligned currents are located in a narrow band of $\sim$1 R_E in the GSM **x**–**y**-plane and extend over several hours MLT in the postnoon sector at the magnetopause. The GSM **y**–**z**-plane representation shows that the y–z extent of the FTE can be identified with $\sim$4 R_E in the y direction and $\sim$2 R_E in the z direction. It can also be seen that Cluster is at the outer edge of the FTE structure.

[87] Figure 11 also shows the total magnetic field strength in the GSM **y**–**z**-plane. Here two clearly defined patches of

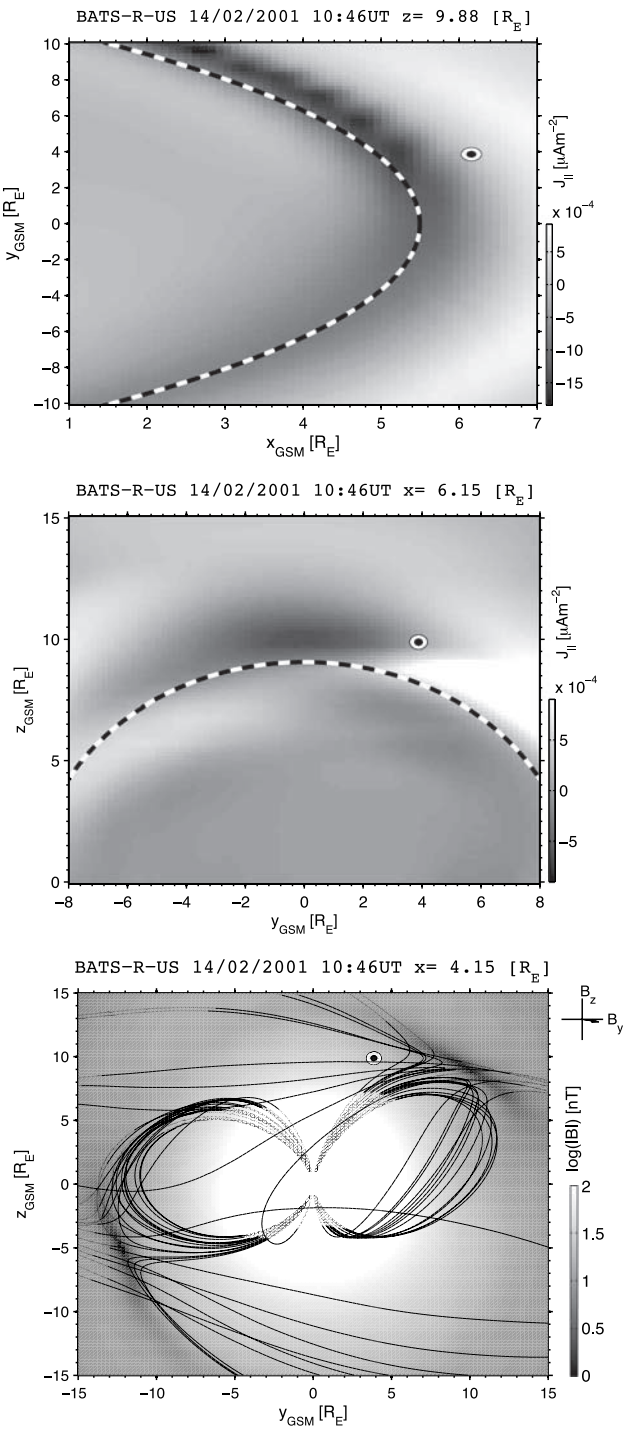

Figure 11. (top and middle) The field-aligned current density sheets at the z and x position of Cluster 1, respectively, in a GSM reference frame at 1046 UT on the 14 February 2001, obtained from a BATS-R-US run. Overlaid on Figures 11 (top) and 11 (bottom) is the magnetopause boundary after *Shue et al.* [1997] in the corresponding planes (indicated by the white/black dashed lines). (bottom) The total magnetic field strength $|B|$ on a logarithmic scale. Overlaid is the MHD-derived magnetic field line topology (black lines) obtained from the Cooling model traces. Overlaid on all three plots is the Cluster 1 position indicated by the white/black dot.

low magnetic field strength (cf. high plasma beta: Figure 8, left) in the Northern and Southern Hemisphere can be observed, these patches are closely related to the reduced shielding effect due to the magnetospheric ''holes'' as described by *Crooker and Siscoe* [1990]. These patches are located directly in the gap between the open and closed field line topology (cf. Figure 9) and indicate the Northern and Southern Hemisphere reconnection site counterparts as outlined by *Crooker* [1979] and *Luhmann et al.* [1984] for antiparallel merging. Overlaid on the total magnetic field strength slice are the MHD-derived field lines mapped from the Cooling traces. The shown field line configuration results from a mapping of the Cooling traces which intersect the presented $\mathbf{y}-\mathbf{z}$-slice plane for the Cluster location and fulfill the conditions; $x = 4.15 \pm 2\ R_E$, and coincide with the two low magnetic field strength regions.

[88] With these information we are able to model the full three-dimensional view of the field line topology. Figure 12 shows the three-dimensional magnetic field line configuration just after reconnection took place (for the 1046 UT event). Using the Cooling model traces of the points at which the flux tubes thread the magnetopause and the MHD simulation, we are able to trace the field lines connected to the Northern and Southern Hemispheres, respectively. We have marked exemplarily those in close proximity to Cluster and fulfilling the condition mentioned above in red as well as the counterparts in the Southern Hemisphere. In order to identify the Southern Hemisphere field lines, we have used points from the Cooling model traces in the Southern Hemisphere which coincide with the low magnetic field strength areas in Figure 11 (third frame) and have then chosen three field lines as examples.

[89] The light gray lines represent the magnetic field lines mapped from a $15^\circ \times 15^\circ$ latitude-longitude grid of the Earth at 100 km altitude. The gray scale slices represent the logarithmic kinetic pressure distribution. The white/black dashed lines indicate the inner magnetopause boundary after *Shue et al.* [1997] and the green isosurfaces represent the plasma cavities above and beneath the neutral sheet as bearing. The modeled field line topology is consistent with the shape and location postulated by *Lockwood and Hapgood* [1998] for the Russell and Elphic type FTE model, and consistent with the open field line topology envisaged by *Dungey* [1961]. Figure 12 shows for the first time the global field line topology for concurrent space- and ground-based observations. The presented topology and especially the red marked field lines show the same features as schematically sketched by *Lockwood and Hapgood* [1998]. From the location of the field lines and the superimposed forces acting on them from the solar wind, a poleward and dawnward motion for the field lines (red) connected to the Northern Hemisphere and duskward and poleward for the ones connected to the Southern Hemisphere can be inferred. These motions would then be consistent with the Northern and Southern Hemisphere ionospheres radar observations.

6. Summary and Conclusions

[90] In this paper we have extended the work of *Daum and Wild* [2006] in order to analyze the three-dimensional large-scale structure and evolution of FTEs utilizing a global MHD simulation combined with in situ space- and ground-based observations. We have revisited the Cluster observations from the 14 February 2001 in the time from 0900 to 1100 UT which were first described by *Wild et al.* [2001]. In the period of interest the Cluster formation was on an outbound pass through the high-latitude postnoon magnetopause during which the magnetic footprint of the spacecraft passed through the field of view of the Finland SuperDARN radar. Space- and ground-based observations have been combined with a global MHD simulation in order to ascertain the large-scale dynamics of the FTEs and the associated reconnection sites.

[91] During the outbound pass the Cluster field and particle instruments showed magnetic disturbances and a mixture of magnetospheric and magnetosheath-like plasma. These perturbations culminated in the observation of four magnetospheric FTEs adjacent to the magnetopause and later the observation of two FTEs during the traversal of the magnetosheath. As indicated by *Wild et al.* [2001, 2003] and *Daum and Wild* [2006], these field and plasma observations are consistent with open flux tubes connected to the Northern Hemisphere which are produced by pulsed reconnection at the dayside magnetopause.

[92] Examination of the radar data at the location of the magnetically mapped Cluster footprint reveals a band of enhanced backscatter between $\sim 74.5^\circ$ to 76.0°N MLAT in close vicinity to the open-closed field line boundary, the flows observed in this band by the SuperDARN radar stations were mainly westward and poleward. Furthermore the flows observed in the band were found to pulse with similar periodicity to the observed FTE signatures in the space-based instruments. The radar observations form classic ''pulsed ionospheric flows'' and ''poleward moving radar auroral forms'' which are believed to be directly linked to the motion of newly opened flux tubes over the polar cap.

[93] Because of the transient nature of the FTE structures, which extend several Earth radii at the magnetopause and several hundred kilometers in the conjugate ionosphere, only a global approach can address the linked sets of objectives concerning the nature of this time-varying phenomenon. The main focus of this paper was to accomplish a direct point-to-point link between the in situ space- and ground-based observations by tracing the FTE signatures from the points of observation in the vicinity of the magnetopause down to the conjugate ionosphere. To accomplish this, we used the BATS-R-US global MHD code in combination with a simple flux tube motion model (Cooling) to investigate the large-scale properties (evolution, location, orientation, and spatial extend) of the reconnection sites involved in the formation of the FTEs and subsequently the FTE features observed. The Cooling model was used to track the motion of the FTEs over the magnetopause. The locus of points where the FTE threads the magnetopause was then used to produce three-dimensional views of the general field line topologies exploiting the high-resolution MHD data. From these topologies and the field-aligned current densities obtained from the MHD model, the location of the reconnection sites has been inferred. The reconnection locations suggested by the MHD model were in good agreement with previous theoretical studies undertaken by *Penz et al.* [2006a] and *Penz* [2006] for the same period of interest.

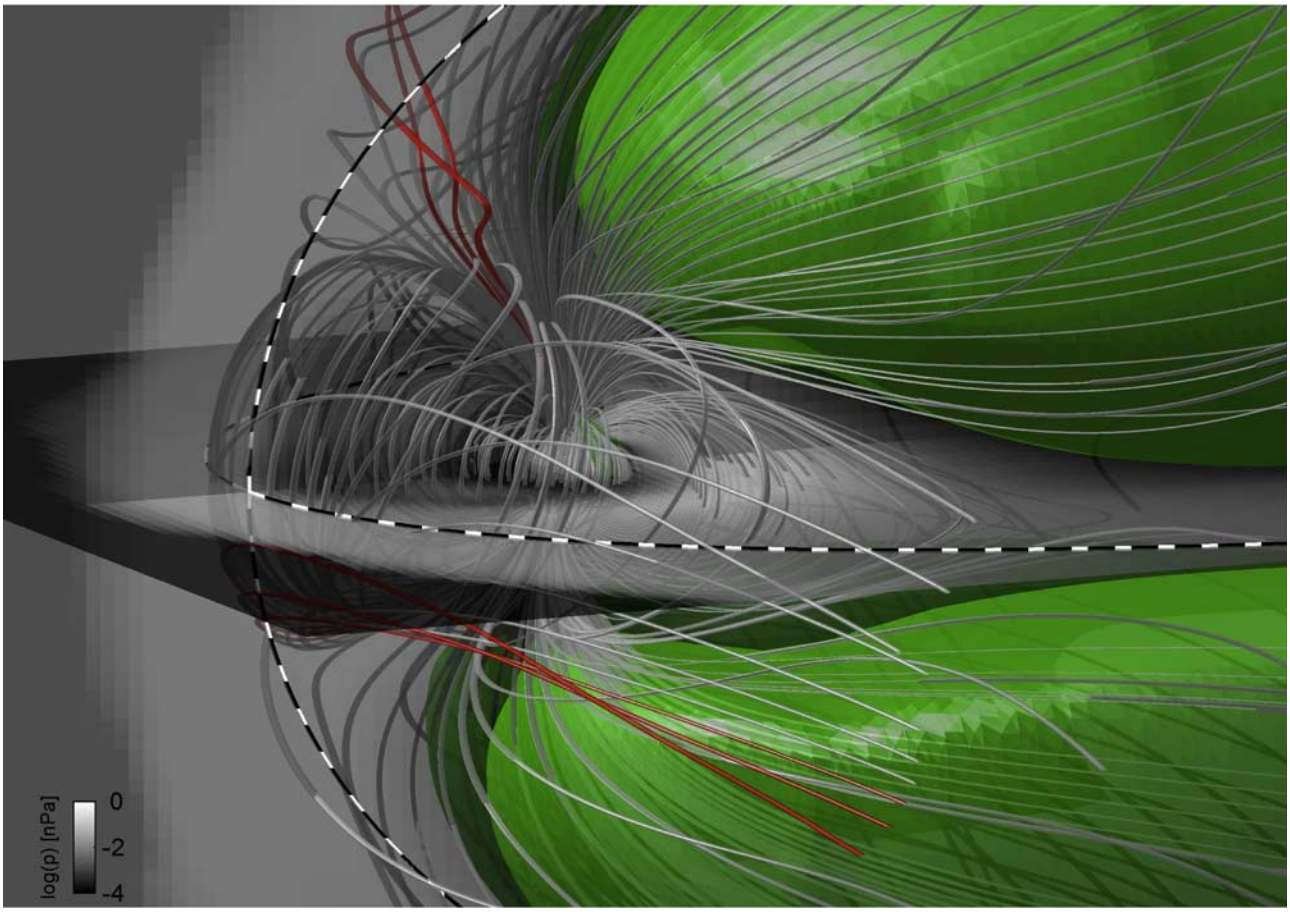

Figure 12. Three-dimensional representation of the magnetic field line topology derived from the BATS-R-US MHD model run for the 14 February 2001 at 1046 UT. The solid light gray lines indicate the magnetic field line configuration mapped from a $15^\circ \times 15^\circ$ geographical latitude-longitude grid on the Earth at 100 km altitude. The red lines indicate the open magnetic field line mappings obtained from the Cluster position for the Northern Hemisphere and the Cooling model for the Southern Hemisphere. The gray scale-coded slices indicate the kinetic pressure distribution obtained from the BATS-R-US model. The green isosurfaces represent the plasma cavities above and beneath the neutral sheet. The magnetopause boundary after *Shue et al.* [1997] is indicated by the white/black dashed lines.

[94] Using the FTE traces given by the Cooling model in combination with the MHD simulation, we were then able to trace the motion of the newly opened flux tubes from the magnetopause down to the conjugate ionosphere at an altitude of 100 km. Here, the modeled traces show good correlation with the LOS data of the SuperDARN radar system with a clear indicated motion westward and poleward as originally outlined by *Wild et al.* [2003].

[95] The MHD model suggests an antiparallel merging scheme topology as predicted by the characterization of *Park et al.* [2006] for mainly southward ($B_z < 0$) and dawnward ($B_y > 0$) IMF conditions, as present at the times of observation. The reconnection sites seen in the model extend about 3.5 h MLT in the postnoon high-latitude magnetopause in a narrow band of $\sim$1 R_E following the shape of the magnetopause. We should note here that due to the time resolution of the MHD run (1 min) this antisunward transient could only be observed in very limited form due to the ''snapshot'' nature of the MHD modeling technique.

[96] It should be noted that the reconnection site locations in the MHD models and discussed here are directly dependent upon the resistivity used in the model [*Berchem et al.*, 2008]. Too low resistivity could lead to neglecting the component merging. However the study of *Park et al.* [2006] shows that the antiparallel merging would be predominant under the present IMF conditions so that we are confident in neglecting the component merging here. It also shows that even with a global model and in situ observation it is still difficult to decide which merging scheme is responsible for the observations. We have shown that the features which arose from the antiparallel merging topology present in the model data show a good correlation with the in situ observations. A conclusive answer to whether antiparallel or component merging is responsible for the observed features can therefore still not be given and will be scrutinized in further studies using simultaneous observations of the Northern and Southern Hemisphere (e.g., during intervals with greater availability of ionospheric flow measurements).

[97] We have demonstrated that the synergy of localized observations and global modeling presents a powerful and unique technique to investigate the large-scale dynamics of the coupling between the solar wind and the magnetosphere exploiting space- and ground-based instruments as well as global MHD simulation. This allows us to put the localized observations in a global context and follows the objectives first outlined by *Berchem* [2000] which are the verification and validation of the models and the identification of the dynamics of large-scale processes in the geospace environment. Owing to the synergy effects of this combination, we were able to unite into one study several individual study results which addressed distinct observational and characteristic model features of FTEs. This allowed us for the first time to produce a coherent three-dimensional picture of the formation, evolution, and topology of FTEs in combination with concurrent observations of FTEs and ionospheric flow patterns.

[98] While state-of-the-art MHD models can be used to establish causal relationships between the point measurements taken by the instruments and the large-scale dynamics present in the magnetosphere, in order to characterize the small-scale processes identified by the instruments global kinetic simulations are indispensable and will be subject of future studies in the modeling community due to the recent advances in technology and simulations. Although global kinetic models are still a few years from being widely used in the community, first multiscale modeling approaches have developed in order to fill the gap between the small-scale kinetic models and the global simulations. A first approach is described by *Kuznetsova et al.* [2007] and bridges the gap successfully between the two modeling domains, further studies of this kind will follow until the advances in technology will allow the global kinetic models to substitute the currently dominant global MHD simulations. A first approach to these ''global'' kinetic models is described by, e.g., *Gargaté et al.* [2007, 2008]. Here particle-in-cell (PIC) hybrid simulations are used to study space plasma interactions using kinetic ions and fluid electrons. Also here first intermediate steps have developed to combine the MHD and the PIC simulation [e.g., *Sugiyama and Kusano*, 2006; *Sugiyama et al.*, 2007]. Further extensions of these combinational studies of MHD and PIC will then also allow detailed small-scale analyses of phenomena in the geospace environment.

[99] **Acknowledgments.** Initial simulation results have been provided by the Community Coordinated Modeling Center at Goddard Space Flight Center. The CCMC is a multiagency partnership between NASA, AFMC, AFOSR, AFRL, AFWA, NOAA, NSF, and ONR. Further runs have been performed on the Lancaster University HPC; the facility is SRIF-funded. PD also thanks M. Pacey for his support and help during the process of installing the SWMF on the Lancaster HPC and his help during the model runs. We would like to thank the model developers at the Center for Space Environment Modeling (CSEM) for their input and help with the model data. We would like to thank all PIs of the instruments employed in this study and the data archive curators. The ACE satellite Level 2 data employed in this study was obtained through the Coordinated Data Analysis Web (CDAWeb). The ESA Cluster data was obtained trough the Cluster Active Archive web interface. We would like to thank all SuperDARN PIs who provided radar data. We thank A. Chulaki and L. Rastätter who provided us with data and deeper insight of the global MHD model. PD was supported by a Lancaster University studentship. TP was supported by the Marie Curie Fellowship contract MTKD-CT-2004-002769 of the project ''The influence of stellar high radiation on planetary atmospheres.'' ML was supported by STFC grant PP/E/000983.

[100] Amitava Bhattacharjee thanks Michael A. Hapgood and another reviewer for their assistance in evaluating this paper.

References

Balogh, A., et al. (1997), The Cluster magnetic field investigation, *Space Sci. Rev.*, *79*(1–2), 65–91, doi:10.1023/A:1004970907748.

Balogh, A., et al. (2001), The Cluster Magnetic Field Investigation: Overview of in-flight performance and initial results, *Ann. Geophys.*, *19*, 1207–1217.

Bennett, L., M. G. Kivelson, K. K. Khurana, L. A. Frank, and W. R. Paterson (1997), A model of the Earth's distant bow shock, *J. Geophys. Res.*, *102*(A12), 26,927–26,942, doi:10.1029/97JA01906.

Berchem, J. (2000), Global MHD Simulations for Cluster-II, in *Proceedings of the Cluster-II Workshop: Multiscale/Multipoint Plasma Measurements*, *Eur. Space Agency Spec. Publ.*, *ESA SP-449*, 211–217.

Berchem, J., and R. Richard (2007), Large-scale topology of magnetic reconnection at the dayside magnetopause: Results from global simulations, *Geophys. Res. Abs.*, *9*, 05840.

Berchem, J., and C. T. Russell (1984), Flux transfer events on the magnetopause: Spatial distribution and controlling factors, *J. Geophys. Res.*, *89*(A8), 6689–6703, doi:10.1029/JA089iA08p06689.

Berchem, J., J. Raeder, and M. Ashour-Abdalla (1995), Magnetic flux ropes at the high-latitude magnetopause, *Geophys. Res. Lett.*, *22*(10), 1189–1192, doi:10.1029/95GL01014.

Berchem, J., et al. (2008), Reconnection at the dayside magnetopause: Comparisons of global MHD simulation results with Cluster and Double Star observations, *J. Geophys. Res.*, *113*, A07S12, doi:10.1029/2007JA012743.

Cagniard, L. (1962), *Reflection and Refraction of Progressive Seismic Waves*, translated from French by E. A. Flinn and C. H. Dix, Gauthier-Villars, Paris.

Chisham, G., et al. (2007), A decade of the Super Dual Auroral Radar Network (SuperDARN): Scientific achievements, new techniques and future directions, *Surv. Geophys.*, *28*(1), 33–109, doi:10.1007/s10712-007-9017-8.

Cooling, B. M. A., C. J. Owen, and S. J. Schwartz (2001), Role of the magnetosheath flow in determining the motion of open flux tubes, *J. Geophys. Res.*, *106*(A9), 18,763–18,776, doi:10.1029/2000JA000455.

Cowley, S. W. H. (1973), A qualitative study of the reconnection between the Earth's magnetic field and an interplanetary field of arbitrary orientation, *Radio Sci.*, *8*(11), 903–913, doi:10.1029/RS008i011p00903.

Cowley, S. W. H. (1976), Comments on the merging of nonantiparallel magnetic fields, *J. Geophys. Res.*, *81*(19), 3455–3458, doi:10.1029/JA081i019p03455.

Cowley, S. W. H., and M. Lockwood (1992), Excitation and decay of solar wind-driven flows in the magnetosphere-ionosphere system, *Ann. Geophys.*, *10*, 103–115.

Cowley, S. W. H., and C. J. Owen (1989), A simple illustrative model of open flux tube motion over the dayside magnetopause, *Planet. Space Sci.*, *37*(11), 1461–1475, doi:10.1016/0032-0633(89)90116-5.

Crooker, N. U. (1979), Dayside merging and cusp geometry, *J. Geophys. Res.*, *84*(A3), 951–959, doi:10.1029/JA084iA03p00951.

Crooker, N. U., and G. L. Siscoe (1990), On mapping flux transfer events to the ionosphere, *J. Geophys. Res.*, *95*(A4), 3795–3799, doi:10.1029/JA095iA04p03795.

Daly, P. W., D. J. Williams, C. T. Russell, and E. Keppler (1981), Particle signature of magnetic flux transfer events at the magnetopause, *J. Geophys. Res.*, *86*(A3), 1628–1632, doi:10.1029/JA086iA03p01628.

Daum, P. (2007), VisAn MHD: A toolbox in Matlab for MHD computer model data visualisation and analysis, *Ann. Geophys.*, *25*, 779–784.

Daum, P., and J. A. Wild (2006), MHD models for multi-spacecraft/ground-based analysis and conjunction visualisations, in *Numerical Modeling of Space Plasma Flows*, edited by N. V. Pogorelov and G. P. Zank, pp. 125–130, Astron. Soc. of Pac., San Fransisco, Calif.

De Hoffmann, F., and E. Teller (1950), Magneto-hydrodynamic shocks, *Phys. Rev.*, *80*(4), 692–703, doi:10.1103/PhysRev.80.692.

De Hoop, A. T. (1960), A modification of Cagniard's method for solving seismic pulse problems, *App. Sci. Res.*, *8*, 349–356.

De Hoop, A. T. (1961), Theoretical determination of the surface motion of a uniform elastic half-space produced by a dilatational, impulsive, point source, paper presented at Colloque International 111, Cent. Natl. de la Rech. Sci., Marseille, France.

De Zeeuw, D. L., S. Sazykin, R. A. Wolf, T. I. Gombosi, A. J. Ridley, and G. Tóth (2004), Coupling of a global MHD code and an inner magnetospheric model: Initial results, *J. Geophys. Res.*, *109*, A12219, doi:10.1029/2003JA010366.

Dubinin, E. M., I. M. Podgornyi, and I. N. Potanin (1980), Structure of the magnetic field at the boundary of the magnetosphere (Analysis of a simulation experiment), *Cosmic Res.*, *18*, 77–87.

Dungey, J. W. (1961), Interplanetary magnetic field and the auroral zones, *Phys. Rev. Lett.*, *6*, 47–48, doi:10.1103/PhysRevLett.6.47.

Dunlop, M. W., D. J. Southwood, K.-H. Glassmeier, and F. M. Neubauer (1988), Analysis of multipoint magnetometer data, *Adv. Space Res.*, *8*(9–10), 273–277, doi:10.1016/0273-1177(88)90141-X.

Dunlop, M. W., et al. (2005), Coordinated Cluster/Double Star observations of dayside reconnection signatures, *Ann. Geophys.*, *23*, 2867–2875.

Elphic, R. C. (1995), Observations of flux transfer events: A review, in *Physics of the Magnetopause*, *Geophys. Monogr. Ser.*, vol. 90, edited by P. Song, B. U. Ö. Sonnerup, and M. F. Thomsen, pp. 225–233, AGU, Washington, D. C.

Elphic, R. C., M. Lockwood, S. W. H. Cowley, and P. E. Sandholt (1990), Flux transfer events at the magnetopause and in the ionosphere, *Geophys. Res. Lett.*, *17*(12), 2241–2244, doi:10.1029/GL017i012p02241.

Escoubet, C. P., M. Fehringer, and M. L. Goldstein (2001), The Cluster mission, *Ann. Geophys.*, *19*, 1197–1200.

Fear, R. C., S. E. Milan, A. N. Fazakerley, C. J. Owen, T. Asikainen, M. G. G. T. Taylor, E. A. Lucek, H. Rème, I. Dandouras, and P. W. Daly (2007), Motion of flux transfer events: a test of the Cooling model, *Ann. Geophys.*, *25*, 1669–1690.

Fedder, J. A., S. P. Slinker, J. G. Lyon, and C. T. Russell (2002), Flux transfer events in global numerical simulations of the magnetosphere, *J. Geophys. Res.*, *107*(A5), 1048, doi:10.1029/2001JA000025.

Fu, Z. F., and L. C. Lee (1986), Multiple X line reconnection, 2. The dynamics, *J. Geophys. Res.*, *91*(A12), 13,373–13,383, doi:10.1029/JA091iA12p13373.

Gargaté, L., R. Bingham, R. A. Fonseca, and L. O. Silva (2007), dHybrid: A massively parallel code for hybrid simulations of space plasmas, *Comput. Phys. Commun.*, *176*(6), 419–425, doi:10.1016/j.cpc.2006.11.013.

Gargaté, L., R. Bingham, R. A. Fonseca, R. Bamford, A. Thornton, K. Gibson, J. Bradford, and L. O. Silva (2008), Hybrid simulations of mini-magnetospheres in the laboratory, *Plasma Phys. Control. Fusion*, *50*, 074017, doi:10.1088/0741-3335/50/7/074017.

Glassmeier, K.-H., and M. Stellmacher (1996), Mapping flux transfer events to the ionosphere, *Adv. Space Res.*, *18*(8), 151–160, doi:10.1016/0273-1177(95)00983-3.

Gombosi, T. I., D. L. De Zeeuw, K. G. Powell, A. J. Ridley, I. V. Sokolov, Q. F. Stout, and G. Tóth (2003), Adaptive mesh refinement for global magnetohydrodynamic simulation, in *Space Plasma Simulation*, edited by J. Büchner, C. T. Dum, and M. Scholer, *Lecture Notes in Phys.*, vol. 615, pp. 247–274, Springer, Heidelberg, Germany.

Gonzales, W. D., and F. S. Mozer (1974), A quantitative model for the potential resulting from reconnection with an arbitrary interplanetary magnetic field, *J. Geophys. Res.*, *79*(28), 4186–4194, doi:10.1029/JA079i028p04186.

Greenwald, R. A., et al. (1995), DARN/SuperDARN: A global view of the dynamics of high-latitude convection, *Space Sci. Rev.*, *71*(1–4), 761–796, doi:10.1007/BF00751350.

Haerendel, G., G. Paschmann, N. Sckopke, H. Rosenbauer, and P. C. Hedgecock (1978), The frontside boundary layer of the magnetopause and the problem of reconnection, *J. Geophys. Res.*, *83*, 3195–3216.

Hasegawa, H., B. U. Ö. Sonnerup, C. J. Owen, B. Klecker, G. Paschmann, A. Balogh, and H. Rème (2006), The structure of flux transfer events recovered from Cluster data, *Ann. Geophys.*, *24*, 603–618.

Heyn, M. F., and V. S. Semenov (1996), Rapid reconnection in compressible plasma, *Phys. Plasmas*, *3*, 2725–2741, doi:10.1063/1.871723.

Johnstone, A. D., et al. (1997), PEACE: A plasma electron and current instrument, *Space Sci. Rev.*, *79*(1–2), 351–398, doi:10.1023/A:1004938001388.

Kawano, H., and C. T. Russell (1996), Survey of flux transfer events observed with the ISEE 1 spacecraft: Rotational polarity and the source region, *J. Geophys. Res.*, *101*(A12), 27,299–27,308, doi:10.1029/96JA02703.

Kawano, H., and C. T. Russell (1997), Survey of flux transfer events observed with the ISEE 1 spacecraft: Dependence on the interplanetary magnetic field, *J. Geophys. Res.*, *102*(A6), 11,307–11,314, doi:10.1029/97JA00481.

Kawano, H., and C. T. Russell (2005), Dual-satellite observations of the motions of flux transfer events: Statistical analysis with ISEE 1 and ISEE 2, *J. Geophys. Res.*, *110*, A07217, doi:10.1029/2004JA010821.

Khan, H., and S. W. H. Cowley (1999), Observations of the response time of high latitude ionospheric convection to variations in the interplanetary magnetic field using EISCAT and IMP-8 data, *Ann. Geophys.*, *17*, 1306–1335.

Kobel, E., and E. O. Flückiger (1994), A model of the steady state magnetic field in the magnetosheath, *J. Geophys. Res.*, *99*(A12), 23,617–23,622, doi:10.1029/94JA01778.

Kuznetsova, M. M., M. Hesse, L. Rastätter, A. Taktakishvili, G. Tóth, D. L. De Zeeuw, A. Ridley, and T. I. Gombosi (2007), Multiscale modeling of magnetospheric reconnection, *J. Geophys. Res.*, *112*, A10210, doi:10.1029/2007JA012316.

Lee, L. C., and Z. F. Fu (1985), A theory of magnetic flux transfer at the Earth's magnetopause, *Geophys. Res. Lett.*, *12*(2), 105–108, doi:10.1029/GL012i002p00105.

Lee, L. C., and Z. F. Fu (1986), Multiple X line reconnection, 1. A criterion for the transition from a single X line to a multiple X line reconnection, *J. Geophys. Res.*, *91*(A6), 6807–6815, doi:10.1029/JA091iA06p06807.

Lockwood, M., and M. A. Hapgood (1998), On the cause of a magnetospheric flux transfer event, *J. Geophys. Res.*, *103*(A11), 26,453–26,478, doi:10.1029/98JA02244.

Lockwood, M., and M. N. Wild (1993), On the quasi-periodic nature of magnetopause flux transfer events, *J. Geophys. Res.*, *98*(A4), 5935–5940, doi:10.1029/92JA02375.

Luhmann, J. G., R. J. Walker, C. T. Russell, N. U. Crooker, J. R. Spreiter, and S. S. Stahara (1984), Patterns of magnetic field merging sites on the magnetopause, *J. Geophys. Res.*, *89*(A3), 1739–1742, doi:10.1029/JA089iA03p01739.

Lundin, R., and D. S. Evans (1985), Boundary layer plasma as a source for high-latitude, early afternoon, auroral arcs, *Planet. Space Sci.*, *33*(12), 1389–1406, doi:10.1016/0032-0633(85)90115-1.

Marchaudon, A., J.-C. Cerisier, J.-M. Bosqued, M. W. Dunlop, J. A. Wild, P. M. E. Décréau, M. Förster, D. Fontaine, and H. Laako (2004), Transient plasma injections in the dayside magnetosphere: One-to-one correlated observations by Cluster and SuperDARN, *Ann. Geophys.*, *22*, 141–158.

Massetti, S. (2006), Antiparallel magnetic merging signatures during IMF $B_Y \gg 0$: Longitudinal and latitudinal cusp aurora bifurcations, *Ann. Geophys.*, *24*, 2299–2311.

McComas, D. J., S. J. Bame, P. Barker, W. C. Feldman, J. L. Phillips, P. Riley, and J. W. Griffee (1998), Solar Wind Electron Proton Alpha Monitor (SWEPAM) for the Advanced Composition Explorer, *Space Sci. Rev.*, *86*(1–4), 563–612, doi:10.1023/A:1005040232597.

McWilliams, K. A., T. K. Yeoman, J. B. Sigwarth, L. A. Frank, and M. Brittnacher (2001), The dayside ultraviolet aurora and convection responses to a southward turning of the interplanetary magnetic field, *Ann. Geophys.*, *19*, 707–721.

Meng, C.-L., and R. Lundin (1986), Auroral morphology of the midday oval, *J. Geophys. Res.*, *91*(A2), 1572–1584, doi:10.1029/JA091iA02p01572.

Neudegg, D. A., T. K. Yeoman, S. W. H. Cowley, G. Provan, G. Haerendel, W. Baumjohann, U. Auster, K.-H. Fornacon, E. Georgescu, and C. J. Owen (1999), A flux transfer event observed at the magnetopause by the Equator-S spacecraft and in the ionosphere by the CUTLASS HF radar, *Ann. Geophys.*, *17*, 707–711.

Neudegg, D. A., et al. (2000), A survey of magnetopause FTEs and associated flow bursts in the polar ionosphere, *Ann. Geophys.*, *18*, 416–435.

Ogino, T., R. J. Walker, M. Ashour-Abdalla, and J. M. Dawson (1986), An MHD simulation of the effects of the interplanetary magnetic field B_y component on the interaction of the solar wind with the Earth's magnetosphere during southward interplanetary magnetic field, *J. Geophys. Res.*, *91*(A9), 10,029–10,046, doi:10.1029/JA091iA09p10029.

Owen, C. J., et al. (2001), Cluster PEACE observations of electrons during magnetospheric flux transfer events, *Ann. Geophys.*, *19*, 1509–1522.

Park, K. S., T. Ogino, and R. J. Walker (2006), On the importance of antiparallel reconnection when the dipole tilt and IMF B_y are nonzero, *J. Geophys. Res.*, *111*, A05202, doi:10.1029/2004JA010972.

Paschmann, G., G. Haerendel, I. Papamastorakis, N. Sckopke, S. J. Bame, J. T. Gosling, and C. T. Russell (1982), Plasma and magnetic field characteristics of magnetic flux transfer events, *J. Geophys. Res.*, *87*(A4), 2159–2168, doi:10.1029/JA087iA04p02159.

Penz, T. (2006), Reconstruction of reconnection: Theoretical considerations and application to Cluster data, Ph.D. thesis, 87 pp., Univ. of Graz, Austria.

Penz, T., C. J. Farrugia, V. V. Ivanova, V. S. Semenov, S. W. H. Cowley, H. K. Biernat, K. W. Ogilvie, and R. Torbert (2006a), Reconstruction of the reconnection electric field at the dayside magnetopause during FTE activity, in *Proceedings of the 6th International Conference "Problems of Geocosmos", St. Petersburg, May 23–27*, edited by V. N. Troyan, V. S. Semenov, and M. V. Kubyshkina, pp. 151–154, St. Petersburg Univ., Russia.

Penz, T., V. S. Semenov, V. V. Ivanova, H. K. Biernat, V. A. Sergeev, R. Nakamura, I. V. Kubyshkin, I. B. Ivanov, and M. F. Heyn (2006b), A reconstruction method for the reconnection rate applied to Cluster magnetotail measurements, *Adv. Space Res.*, *37*(7), 1388–1393, doi:10.1016/j.asr.2005.05.020.

Penz, T., C. J. Farrugia, V. V. Ivanova, V. S. Semenov, I. B. Ivanov, S. W. H. Cowley, H. K. Biernat, and R. B. Torbert (2007), Modeled variations of the reconnection electric field at the dayside magnetopause during continued flux transfer event activity, *J. Geophys. Res.*, *112*, A01S90, doi:10.1029/2006JA011937.

Pinnock, M., A. S. Rodger, J. R. Dudeney, K. B. Baker, P. T. Newell, R. A. Greenwald, and M. E. Greenspan (1993), Observations of an enhanced convection channel in the cusp ionosphere, *J. Geophys. Res.*, *98*(A3), 3767–3776, doi:10.1029/92JA01382.

Pinnock, M., A. S. Rodger, J. R. Dudeney, F. Rich, and K. B. Baker (1995), High spatial and temporal resolution observations of the ionospheric cusp, *Ann. Geophys.*, *13*, 919–925.

Pitout, F., and P. L. Blelly (2003), Ionospheric response to Flux Transfer Events at the Earth's Magnetopause, in *Proceedings of ICPP 2002: International Congress on Plasma Physics*, edited by I. S. Falconer, J. Khachan and R. L. Dewar, *AIP Conf. Proc.*, *669*, 835–839.

Powell, K. G., P. L. Roe, T. J. Linde, T. I. Gombosi, and D. L. De Zeeuw (1999), A solution-adaptive upwind scheme for ideal magnetohydrodynamics, *J. Comput. Phys.*, *154*(2), 284–309, doi:10.1006/jcph.1999.6299.

Provan, G., and T. K. Yeoman (1999), Statistical observations of the MLT, latitude and size of pulsed ionospheric flows with the CUTLASS Finland radar, *Ann. Geophys.*, *17*, 855–867.

Provan, G., T. K. Yeoman, and S. E. Milan (1998), CUTLASS Finland radar observations of the ionospheric signatures of flux transfer events and the resulting plasma flows, *Ann. Geophys.*, *16*, 1411–1422.

Provan, G., S. E. Milan, M. Lester, T. K. Yeoman, and H. Khan (2002), Simultaneous observations of the ionospheric footprint of flux transfer events and dispersed ion signatures, *Ann. Geophys.*, *20*, 281–287.

Pu, Z. Y., et al. (2006), Cluster and TC1 five point observations of an FTE on January 4, 2005; A preliminary study, in *Proceedings Cluster and Double Star Symposium - 5th Anniversary of Cluster in Space*, *Eur. Space Agency Spec. Publ.*, *ESA SP-598*, 5–1.4.

Raeder, J. (2006), Flux transfer events: 1. Generation mechanism for strong southward IMF, *Ann. Geophys.*, *24*, 381–392.

Rème, H., et al. (1997), The Cluster Ion Spectrometry (CIS) Experiment, *Space Sci. Rev.*, *79*(1–2), 303–350, doi:10.1023/A:1004929816409.

Rème, H., et al. (2001), First multispacecraft ion measurements in and near the Earth's magnetosphere with the identical Cluster ion spectrometry (CIS) experiment, *Ann. Geophys.*, *19*, 1303–1354.

Ridley, A. J., and M. W. Liemohn (2002), A model-derived storm time asymmetric ring current driven electric field description, *J. Geophys. Res.*, *107*(A8), 1151, doi:10.1029/2001JA000051.

Ridley, A. J., T. I. Gombosi, and D. L. De Zeeuw (2004), Ionospheric control of the magnetosphere: Conductance, *Ann. Geophys.*, *22*, 567–584.

Rijnbeek, R. P., S. W. H. Cowley, D. J. Southwood, and C. T. Russell (1984), A survey of dayside flux transfer events observed by ISEE-1 and -2 magnetometers, *J. Geophys. Res.*, *89*(A2), 786–800, doi:10.1029/JA089iA02p00786.

Robert, P., O. Lecontel, A. Roux, P. Canu, D. Fontaine, G. Chanteur, J.-M. Bosqued, C. J. Owen, A. N. Fazakerley, and M. W. Dunlop (2006), Study of a flux transfer event with Cluster spacecraft, in *Proceedings Cluster and Double Star Symposium - 5th Anniversary of Cluster in Space*, *Eur. Space Agency Spec. Publ.*, *ESA SP-598*, 5–1.6.

Rodger, A. S., and M. Pinnock (1997), The ionospheric response to FTEs: The first few minutes, *Ann. Geophys.*, *15*, 685–691.

Roe, P. L. (1981), Approximate Riemann solvers, parameter vectors, and difference schemes, *J. Comput. Phys.*, *43*(2), 357–372, doi:10.1016/0021-9991(81)90128-5.

Ruohoniemi, J. M., and K. B. Baker (1998), Large-scale imaging of high-latitude convection with Super Dual Auroral Radar Network HF radar observations, *J. Geophys. Res.*, *103*(A9), 20,797–20,811, doi:10.1029/98JA01288.

Ruohoniemi, J. M., and R. A. Greenwald (1996), Statistical patterns of high-latitude convection obtained from Goose Bay HF radar observations, *J. Geophys. Res.*, *101*(A10), 21,743–21,764, doi:10.1029/96JA01584.

Russell, C. T., and R. C. Elphic (1978), Initial ISEE magnetometer results: Magnetopause observations, *Space Sci. Rev.*, *22*(6), 681–715, doi:10.1007/BF00212619.

Russell, C. T., and R. C. Elphic (1979), ISEE observations of flux transfer events at the dayside magnetopause, *Geophys. Res. Lett.*, *6*(1), 33–36, doi:10.1029/GL006i001p00033.

Russell, C. T., J. Berchem, and J. G. Luhmann (1985), On the source regions of flux transfer events, *Adv. Space Res.*, *5*(4), 363–368, doi:10.1016/0273-1177(85)90162-0.

Šafránková, J., Z. Nemeèek, Š. Dušík, L. Přeck, D. G. Sibeck, and N. N. Borodkova (2002), The magnetopause shape and location: A comparison of the Interball and Geotail observations with models, *Ann. Geophys.*, *20*, 301–309.

Sandholt, P. E., M. Lockwood, T. Oguti, S. W. H. Cowley, K. S. C. Freeman, B. Lybekk, A. Egeland, and D. M. Willis (1990), Midday auroral breakup events and related energy and momentum transfer from the magnetosheath, *J. Geophys. Res.*, *95*(A2), 1039–1060, doi:10.1029/89JA00817.

Sandholt, P. E., C. J. Farrugia, and W. F. Denig (2004), Detailed dayside auroral morphology as a function of local time for southeast IMF orientation: Implications for solar wind-magnetosphere coupling, *Ann. Geophys.*, *22*, 3537–3560.

Saunders, M. (1989), The Polar cusp ionosphere: A window on solar wind-magnetosphere coupling, *Antarct. Sci.*, *1*(3), 193–203, doi:10.1017/S0954102089000313.

Scholer, M., D. Hovestadt, F. M. Ipavich, and G. Gloeckler (1982), Energetic protons, alpha particles, and electrons in the magnetic flux transfer events, *J. Geophys. Res.*, *87*(A4), 2169–2175, doi:10.1029/JA087iA04p02169.

Semenov, V. S., T. Penz, V. V. Ivanova, V. A. Sergeev, H. K. Biernat, R. Nakamura, M. F. Heyn, I. V. Kubyshkin, and I. B. Ivanov (2005), Reconstruction of the reconnection rate from Cluster measurements: First results, *J. Geophys. Res.*, *110*, A11217, doi:10.1029/2005JA011181.

Shue, J.-H., J. K. Chao, H. C. Fu, C. T. Russell, P. Song, K. K. Khurana, and H. J. Singer (1997), A new functional form to study the solar wind control of the magnetopause size and shape, *J. Geophys. Res.*, *102*(A5), 9497–9512, doi:10.1029/97JA00196.

Smith, C. W., J. L'Heureux, N. F. Ness, M. H. Acuña, L. F. Burlaga, and J. Scheifele (1998), The ACE Magnetic Fields Experiment, *Space Sci. Rev.*, *86*(1–4), 613–632, doi:10.1023/A:1005092216668.

Smith, M. F., and C. J. Owen (1992), Temperature anisotropies in a magnetospheric FTE, *Geophys. Res. Lett.*, *19*(19), 1907–1910, doi:10.1029/92GL01618.

Sonnerup, B. U. Ö. (1970), Magnetic-field reconnection in a highly conducting incompressible fluid, *J. Plasma Phys.*, *4*, 161–174.

Sonnerup, B. U. Ö. (1974), The magnetopause reconnection rate, *J. Geophys. Res.*, *79*(10), 1546–1549, doi:10.1029/JA079i010p01546.

Sonnerup, B. U. Ö., and L. J. Cahill Jr. (1967), Magnetopause structure and attitude from Explorer 12 observations, *J. Geophys. Res.*, *72*(1), 171–183, doi:10.1029/JZ072i001p00171.

Spreiter, J. R., A. L. Sumers, and A. Y. Alksne (1966), Hydrodynamic flow around the magnetosphere, *Planet. Space Sci.*, *14*, 223–253.

Stone, E. C., A. M. Frandsen, R. A. Mewaldt, E. R. Christian, D. Margolies, J. F. Ormes, and F. Snow (1998), The Advanced Composition Explorer, *Space Sci. Rev.*, *86*(1–4), 1–22, doi:10.1023/A:1005082526237.

Sugiyama, T., and K. Kusano (2007), Multi-scale plasma simulation by the interlocking of magnetohydrodynamic model and particle-in-cell kinetic model, *J. Comput. Phys.*, *227*(2), 1340–1352, doi:10.1016/j.jcp.2007.09.01.

Sugiyama, T., K. Kusano, S. Hirose, and A. Kageyama (2006), MHD-PIC connection model in a magnetosphere-ionosphere coupling system, *J. Plasma Phys.*, *72*(6), 945–948, doi:10.1017/S0022377806005356.

Thomsen, M. F., J. A. Stansberry, S. J. Bame, S. A. Fuselier, and J. T. Gosling (1987), Ion and electron velocity distributions within flux transfer events, *J. Geophys. Res.*, *92*(A11), 12,127–12,136, doi:10.1029/JA092iA11p12127.

Thorolfsson, A., J.-C. Cerisier, M. Lockwood, P. E. Sandholt, C. Senior, and M. Lester (2000), Simultaneous optical and radar signatures of poleward-moving auroral forms, *Ann. Geophys.*, *18*, 1054–1066.

Toffoletto, F. R., T. W. Hill, and P. H. Reiff (1990), A model of FTE footprints in the polar cap, in *Physics of Magnetic Flux Ropes*, *Geophys. Monogr. Ser.*, vol. 58, edited by C. T. Russell, E. R. Priest, and L. C. Lee, pp. 599–603, AGU, Washington, D. C.

Toffoletto, F. R., S. Sazykin, R. Spiro, and R. Wolf (2003), Inner magnetospheric modeling with the Rice Convection Model, *Space Sci. Rev.*, *107*(1–2), 175–196, doi:10.1023/A:1025532008047.

Tóth, G., et al. (2005), Space Weather Modeling Framework: A new tool for the space science community, *J. Geophys. Res.*, *110*, A12226, doi:10.1029/2005JA011126.

Trattner, K. J., S. M. Petrinec, W. K. Peterson, S. A. Fuselier, and H. Rème (2006), Tracing the location of the reconnection site from the northern and southern cusps, *J. Geophys. Res.*, *111*, A11211, doi:10.1029/2006JA011673.

Vasyliunas, V. M. (1970), Mathematical models of magnetospheric convection and its coupling to the ionosphere, in *Particles and Fields in the Magnetosphere*, edited by B. M. McCormac, pp. 60–71, Springer, Heidelberg, Germany.

Wild, J. A., et al. (2001), First simultaneous observations of flux transfer events at the high-latitude magnetopause by the Cluster spacecraft and pulsed radar signatures in the conjugate ionosphere by the CUTLASS and EISCAT radars, *Ann. Geophys.*, *19*, 1491–1508.

Wild, J. A., et al. (2003), Coordinated interhemispheric SuperDARN radar observations of the ionospheric response to flux transfer events observed by the Cluster spacecraft at the high-latitude magnetopause, *Ann. Geophys.*, *21*, 1807–1826.

Wild, J. A., et al. (2005), Simultaneous in-situ observations of the signatures of dayside reconnection at the high- and low-latitude magnetopause, *Ann. Geophys.*, *23*, 445–460.

Wild, J. A., S. E. Milan, J. A. Davies, M. W. Dunlop, D. M. Wrigth, C. M. Carr, A. Balogh, H. Rème, A. N. Fazakerley, and A. Marchaudon (2007), On the location of dayside magnetic reconnection during an interval of duskward oriented IMF, *Ann. Geophys.*, *25*, 219–239.

Wilken, B., et al. (1997), RAPID: The Imaging Energetic Particle Spectrometer on Cluster, *Space Sci. Rev.*, *79*(1–2), 399–473, doi:10.1023/A:1004994202296.

Wilken, B., et al. (2001), First results from the RAPID imaging energetic particle spectrometer on board Cluster, *Ann. Geophys.*, *19*, 1355–1366.

Wiltberger, M., R. S. Weigel, M. Gehmeyr, and T. Guild (2005), Analysis and visualization of space science model output and data with CISM-DX, *J. Geophys. Res.*, *110*, A09224, doi:10.1029/2004JA010956.

P. W. Daly, Max Planck Institute for Solar System Research, D-37189 Katlenburg-Lindau, Germany.

P. Daum, J. A. Wild, and E. E. Woodfield, Department of Communication Systems, Lancaster University, Lancaster, LA1 4WA UK. (p.daum@lancaster.ac.uk)

A. N. Fazakerley, Department of Space and Climate Physics, Mullard Space Science Laboratory, University College London, Holmbury St. Mary, Dorking, RH5 6NT UK.

M. Lester, Department of Physics and Astronomy, University of Leicester, Leicester, LE1 7RH UK.

T. Penz, Osservatorio Astronomico di Palermo, INAF, I-90134 Palermo, Italy.

H. Rème, Centre d'Etude Spatiale des Rayonnements, F-31028 Toulouse, France.